Unit of Food Microbiology
Institute of Food Safety, Food Technology and Veterinary Public Health
University of Veterinary Medicine Vienna
(Head: Univ.-Prof. Dr.med.vet. Martin Wagner, Dipl.ECVPH)

Coronavirus induced changes in mouse pathophysiology

Master´s thesis

University of Veterinary Medicine Vienna

submitted by
Patrizia Gibler, BSc

Vienna, July 2022

Internal supervision: Priv.-Doz. Dr. rer.nat. Kathrin Kober-Rychli

External supervision: Priv.-Doz Dr. Philipp Hohensinner

Medical University Vienna, Center for Biomedical Research

Reviewer: Assoc.Prof. MMag. Dr.rer.nat. Alice Assinger

Acknowledgments

I want to thank my supervisor Priv.-Doz. Dr. Philipp Hohensinner, for giving me the opportunity to work in this friendly and supportive environment at the Division for Cardiology at the Department of Medicine II in the Anna-Spiegel Research Center. He supported me in all steps of my thesis, always took time for discussions and came up with wonderful ideas for further experiments and setups. He believed in me, encouraged me to attend a scientific congress and present my results there and to continue my education in research.

I also want to thank my supervisor Priv.-Doz. Dr. Kathrin Kober-Rychli form the Unit of Food Microbiology, Institute of Food Safety, Food Technology and Veterinary Public Health at the University of Veterinary Medicine, for supporting me during the writing process and raising my confidence in writing this thesis by giving professional advice.

Further, I want to thank Ao.Univ.-Prof. Dr. Johann Wojta and the Ludwig Bolzmann Institute for Cardiovascular Research for financing my work and making this thesis possible.

A big thank you goes to Manuel Salzmann PhD, who always had time for me, regardless of his workload. He explained everything in detail and completely understandable and taught me many new methods, techniques and programs. He became a very good friend, who always motivates me and made work a place where I felt very comfortable and happy to be.

I want to thank all the other lab members, Mira Brekalo, Frieda Marka MSc., Romana Sickha BBSc., Julia Pointner PhD and Dr. med. Univ. Patrick Haider who helped and supported me and discussed ideas. You all made this laboratory and the working atmosphere so special to me. Thank you, Mira, for making the prettiest stainings and teaching me how to do them. Thank you, Frieda and Romana, for becoming very good friends and supporting me and thanks to Julia and Patrick for explaining, teaching and helping me.

Finally, I want to thank my family and friends. Thank you, mum and dad, as well as my grandparents, for supporting me not only financially but also emotionally and for motivating me in every step of my education. Thanks to Patrick for always having time to talk and being a great brother and thanks to my boyfriend Philip who always supports me, motivates me and is there for me.

Table of Contents

Acknowledgments III
Abstract VI
1 Introduction 1
1.1 Coronavirus 1
1.2 Murine hepatitis virus 2
1.3 C57BL/6J mice 2
1.4 Immune system and response to virus infection 3
1.5 Neutrophils and Neutrophil Extracellular Traps 4
1.7 Effects of Coronavirus to Lung and Liver 5
1.8 Coagulation and Fibrinolytic System 6
1.9 Body Temperature 9
1.10 Microbiome 10
2 Aim 12
3 Methods 13
3.1 qPCR virus burden lung and liver 13
3.1.1 RNA isolation 13
3.1.2 cDNA 13
3.1.3 qPCR 13
3.2 Immunohistochemistry - CitH4 staining lung and liver 14
3.2.1 Scanning of CitH4 stained slides and analysis 15
3.3 qPCR inflammatory markers and PAI, PLG, uPA 15
3.4 Organ culture 16
3.4.1 Culturing liver 16
3.4.2 cDNA 17
3.4.3 qPCR 17
3.5 Trichrome staining collagen 18
3.5.1 Scanning of Trichrome stained slides and analysis 18
3.6 Flow cytometry for low dose infection 19
3.6.1 Lung preparation 19
3.6.2 Flow cytometry 19
3.7 Temperature measurement with an infrared camera 20

3.8 Microbiome analysis of the Altered Schaedler Flora 21
3.9 qPCR analysis and Graphs 22
4 Results 23
4.1 Virus infection and NET formation in the lung 23
4.2 Virus infection and NET formation in the liver 24
4.3 Inflammation markers in liver 26
4.4 Coagulation and Fibrinolysis 28
4.5 Organ culture 28
4.6 Collagen in Lung and Liver 31
4.7 Low concentration MCoV infection 32
4.8 Comparing temperature to weight loss during a MCoV infection 33
4.9 Comparing the ASF of healthy and MCoV infected mice 35
4.10 Comparing the ASF of the AST and Quarantine mice 36
5 Discussion 38
6 Summary English 41
7 Summary German 42
8 List of Abbreviations 43
9 Summary of References 44
10 Summary of Figures 47
11 Summary of Tables 48

Abstract

The main research topic of this master thesis is the analysis of host-pathogen interactions during a coronavirus infection. C57BL/6 mice were intranasally infected with the murine coronavirus (MCoV), which belongs to the same subgroup of betacoronaviruses as the human severe acute respiratory syndrome coronavirus type 2 (SARS-CoV-2) and is therefore a great model to translate findings in our mouse model to the human situation. Moreover, the model was sensitive enough that even a low dose virus infection resulted in a rapid influx of T-cells as well as macrophages in the lung, even though virus burden was not any more detectably. The hypothesis was, that the interaction between the murine coronavirus and its host results in changes in the body temperature, microbiome and a prolonged prothrombotic and inflammatory response.

We observed differences in virus burden and presence of neutrophil extracellular trap (NET) derived thrombi between the lung and the liver. Lung virus burden was highest at day 2 with thrombi at day 10, whereas in the liver the virus burden was highest at day 4 with high thrombus numbers at day 2 and 10. qPCR analysis of inflammation markers of liver mRNA, like tumor necrosis factor alpha (TNFα), interferon gamma (IFNγ), or intracellular adhesion molecule 1 (ICAM-1) revealed that the highest inflammatory response could be seen at day 4. Moreover, collagen deposits in the lung were highest at day 4, whereas liver collagen was highest at day 10.

As NET formation is paralleled by coagulation, also the coagulation factors and fibrinolytic players were investigated. Plasminogen activator inhibitor 1 (PAI-1) and urokinase plasminogen activator (uPA) mRNA were upregulated on day 4, which coincided with high plasma protein levels of TNFα and IFNγ. The induction of uPA and PAI-1 by these cytokines was confirmed in an *ex vivo* liver stimulation model. In line with the *in vivo* findings, PAI-1 and uPA mRNA were again increased in comparison to untreated organ culture, indicating that their expression was directly regulated by hepatic inflammation.

Another aim was to identify if the outer body temperature, measured with an infrared camera, is a better indicator than body weight regarding the wellbeing. It could be shown that body weight was more suited as an early marker for wellbeing than the outer body temperature. However, a clear point of no return could be set with the infrared camera, which may support the decision if the animal should be euthanized or not.

The last part of the thesis focused on alterations in the Altered Schaedler Flora (ASF) microbiota, which includes eight specific bacteria represented in the gut microbiome. Significant differences between control and MCoV infected mice as well as between mice from the Anna Spiegel Animal facility, which had SPF conditions, and the Quarantine, where mice were infected with *Murine Norovirus, Pasteurella sp., Helicobacter sp.* and *protozoa* were detected.

In conclusion, we were able to demonstrate differences between the lung and the liver during an infection with MHV, observing the NET formation and inflammatory response. Furthermore our *in vivo* results were in line with *ex vivo* organ culture and we observed changes of the ASF during a virus infection.

1 Introduction

1.1 Coronavirus

The severe acute respiratory syndrome coronavirus 2 (SARS-CoV-2) was first identified in 2019 as a betacoronavirus causing the acute respiratory coronavirus disease 2019 (COVID-19). The highly transmittable viral infection was first found in Wuhan, China, and rapidly spread worldwide. On March 11th, 2020, the World Health Organization (WHO) declared the disease a pandemic. Symptoms can be flu-like but can progress to severe pneumonia, respiratory failure and even death, depending on the immune system and age[1-3]. The virus is transmitted through respiratory droplets, aerosols or contact with contaminated surfaces[3]. By 7th of July 2022, there have been 548,990,094 confirmed COVID-19 cases, including 6,341,637 deaths[4].

SARS-CoV-2 is an enveloped positive-sense, single-stranded RNA virus, consisting of four main structural proteins (the spike, the envelop, the membrane and nucleocapsid) as well as multiple non-structural proteins[5, 6]. The virus can enter the host cell when the enveloped spike protein binds to the angiotensin-converting enzyme 2 (ACE2) receptor[7-9]. After the entry genomic RNA is released into the cytosol where it is translated into replicase proteins called ORF1a and ORF1b. Resulting polyproteins called pp1a and pp1b get cleaved by a protease into individual replicase complex nonstructural proteins forming the virus replication and transcription complex. Double-membrane vesicles, open double-membrane spherules and convoluted membranes form a protective microenvironment for RNA replication and transcription. Translated proteins translocate into the endoplasmic reticulum (ER) and go through ER and Golgi complex where they finally bud off into the lumen and are secreted from the infected cell by exocytosis[8, 9].

The betacoronaviurs, belonging to the coronaviridae family, which can be seen in Fig.1, consist of four subgenera of which one is embecovirus, which includes SARS-CoV, SARS-CoV-2 and the murine hepatitis virus (MHV)[1, 10].

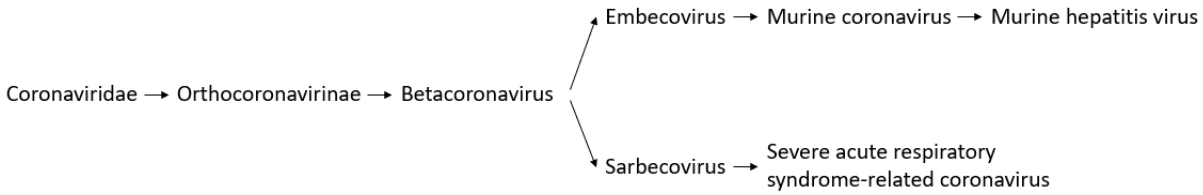

Figure 1: Coronaviridae taxonomy[11].

1.2 Murine hepatitis virus

The murine hepatitis virus (MHV) was first isolated 1949 and is a natural, highly abundant pathogen in mice (*Mus musculus*)[12, 13]. It is the most intensely studied animal coronavirus and perfect for studying the pathogenesis and virulence as well as the immune response. It only requires biosafety level two not level three as SARS-CoV-2 [1]. MHV strains infect either the upper respiratory or the enteric mucosa but they can also spread to other organs, including the liver. MHV-A59 or MCoV, as used in this work, is a respiratory strain and replicates in the nasal respiratory and olfactory epithelium and disseminates among other organs to the lung and liver[1, 13-15]. MHV is a very contagious virus in laboratory mice and can be transmitted by direct contact with infected mice, up to 30 days after infection whereas virus clearance starts one week after infection and elimination withing three to four weeks[14, 16-18]. In general, the duration of infection varies depending on the murine coronavirus strain, immunocompetence, passive immunity, age, genetic strain and genetic alterations[1, 13]. Mice that recover from an MCoV infection are resistant to reinfection with this specific strain[19, 20]. The innate immune system is a strong barrier against a MCoV infection. To fight the corona virus infection, a well-regulated balance between early activation of the innate immune system and controlling the immune system to fight the virus and prevent organ damage is important[13, 21]. Essential for host defense are interferons (IFNs) and their downstream targets which have antiviral, immunomodulating and anti-proliferative effects[13, 22]. After the first encounter with the virus, type one IFNs including IFNα and IFNβ are secreted from cells. To counteract IFN response and signaling in the host MCoV was described to inhibit especially IFNβ[13, 23, 24].

1.3 C57BL/6J mice

To observe the organ specific changes and the immune response caused by MHV, C57Bl/6J mice were used as animal models. C57BL/6J mice are one of the most widely used inbred strain and was the first strain whose genome has been sequenced. The strain was created by Dr. CC Little by mating 57 females with 52 males from Miss Abbie Lathrop´s stock. It is a general-purpose strain and widely used in many arears of research including cardiovascular biology, diabetes and obesity, genetics, neurobiology, developmental biology and sensorineural research. The strain is also used to produce transgenic mice. C57BL/6J mice are long-lived, and breed well, and they have a low susceptibility to tumors[25]. The immune response is characterized by a skewing towards the Th1 direction[26].

1.4 Immune system and response to virus infection

Due to specific pathogen recognition receptors (PRR) the general anti-viral innate mechanism is active, recognizing "self" and "non-self" via recognition the of viral nucleic acids. The virus enters the cell through binding to a specific receptor. Infected cells produce interferons which consist of interferon genes which are further recognized by the immune system and lead to an immune response. The first line of defense are macrophages, dendritic cells and neutrophils which start the immune reaction[27]. These cells induce an activation of several signaling pathways when their PRR interacts with damage associated molecular patterns (DAMPs) or pathogen associated molecular patterns (PAMPs) leading to the production of anti-viral cytokines including type 1 interferons, IFNα and IFNγ and pro-inflammatory cytokines including interleukin-1β (IL-1β), interleukin-6 (IL-6), and tumor necrosis factor alpha (TNFα). Moreover, innate immune cells like neutrophils and natural killer cells reduce the viral load[28]. Integrins expressed on endothelial cells, e.g. intracellular adhesion molecule-1 (ICAM-1) and vascular cell adhesion molecule-1 (VCAM-1) can be bound by T-cells if the inflammatory response starts and are molecular cues for migration of immune cells to specific sites of infection[29, 30]. They lead to the production of pro-inflammatory and anti-viral cytokines and activate the adaptive immune response which can kill infected cells with the help of CD8+ T-cells[28]. CD8 is expressed on cytotoxic T-cells which bind class 1 major histocompatibility complex (MHC) proteins whereas CD4 is expressed on helper t-cells and regulatory T-cells binding class 2 MHC proteins. Recognizing class 1 MHC proteins helps cytotoxic T-cells identifying any infected cell whereas helper and regulatory T-cells support the immune system[31]. CD4+ T-cells orchestrate the immune response against several pathogens including viruses. They help innate cells, B-cells and CD8+ T-cells[32].

The adaptive immune system aims to directly kill virus infected cells by antigen specific T-cells and neutralize the virus by antigen specific B-cells. Further IFNγ produced by T-cells and natural killer cells help with viral clearance. Memory B-cells and memory T-cells are produced to protect the host against a secondary infection[1, 28].

With the pro inflammatory cytokines also a major involvement of macrophages in the lung was observed. Macrophage Activation Syndrome is described as a major risk factor which contributes to lung inflammation. An overreaction of the immune response can lead to a cytokine storm and further to immune exhaustion[27]. This can lead to organ damage including

the lung, heart, liver and kidney and due to a triggered coagulation system clots can form leading to thrombosis in several organs[28].

1.5 Neutrophils and Neutrophil Extracellular Traps

Neutrophils are the primary immune cells and represent about 60 % of blood leukocytes. They are formed every day, have a short half-life but a high metabolic function and are the first-line guards[33]. They differentiate in the bone marrow where they begin to express effector molecules which are stored in granules and later allow them to induce inflammation and kill microbes. Mature neutrophils migrate form the bone marrow to the tissue[34].

Neutrophils are recruited to sites of infection to kill pathogens like bacteria, viruses and fungi by oxidative burst and phagocytosis. They are activated by Toll-like receptors, chemokine-, cytokine-, G protein-coupled receptors which can stimulate neutrophil extracellular traps (NETs) production[34, 35]. NETs are web-like structures composed of DNA, histones, granular proteins like neutrophil elastase and myeloperoxidase (MPO)[36-38]. NETs primarily trap microbes and debris but uncontrolled NET formation leads to alveolar damage, endothelial injury or bleeding disorders. NET formation is a well-regulated process in which neutrophils undergo morphological alterations due to infections, inflammatory mediators or platelets which result in nuclear membrane rupture. With this rupture DNA and histones are mixed with cytoplasmic granular contents like myeloperoxidase and neutrophil elastase. NET release is on the one hand physiologically beneficial during infections but on the other hand excessive NET production can be harmful and lead to tissue injury and thrombosis[35, 37].

Studies with COVID-19 patients showed that high NET levels are associated with an increased duration of the treatment, prolonged recovery time and a higher mortality in severe pneumonia whereas lower NET levels resulted in better outcomes[37]. Further it was seen that the disbalance between NET formation and degradation is important regarding the pathophysiology of inflammation, coagulopathy, organ damage and immunothrombosis[34].

Thrombosis in COVID-19 patients affects arterial and venous circulation and can lead to acute coronary syndrome, stroke, pulmonary embolism, deep vein thrombosis and microvascular thrombosis. Markers found in patients with severe COVID-19 include circulating cell-free DNA, MPO-DNA complexes or citrullinated histones. Moreover neutrophil-platelet aggregates and neutrophil activation markers can be found[34]. Citrullinated histone H3 and H4 are widely used biomarker for NET formation[38, 39].

NETs play an important role during coagulation as platelets get entangled within the NETs leading to platelet activation and aggregation. They also promote thrombin formation as pro-thrombogenic factors like red blood cells and pro-coagulant molecules like fibrinogen, fibronectin and tissue factor are provided. The histone-DNA backbone is expected to give the stability to the fibrin scaffold in the thrombi[37, 38].

NETs can have pro- and anti-inflammatory effects. Pro-inflammatory effects comprise induction of type I interferons (INFs) and proinflammatory cytokines, promotion of the adaptive immune response and immunothrombosis. Anti-inflammatory effects can occur as NETs trap and cleave pro-inflammatory mediators resulting in a downregulation of inflammation[34]. Moreover, NETs can activate the innate immune system through release of IFN for dendritic cells and macrophages and the adaptive immune system through activation of T-lymphocytes[33].

Platelets can modulate neutrophil function by being an activator through direct contact through the expression of adhesion molecules like ICAM-1 and P-selectin which leads to neutrophil recruitment and activation. In general, platelets adhere to injured blood vessels and due to their high number and privileged position in the blood they can be considered as a major activator during viral infection and injury[34].

1.7 Effects of Coronavirus to Lung and Liver

Histopathological studies showed that additionally to shortness of breath and respiratory symptoms, alveolar-capillary damage, immune cell infiltration, fluid-filled alveoli and fibrin deposition can be observed in the lung after a coronavirus infection. Increased serum levels of MPO-DNA and citrullinated histone H3 can be found as well as massive infiltration of neutrophils to the lung which form NETs and are associated with immunothrombosis and potential drivers of the acute respiratory distress syndrome (ARDS)[34, 36, 40].

In the liver, injuries can be found that might result from viral toxicity or from overproduction of cytokines and NETs[34, 41]. A low platelet count, high neutrophil count, high neutrophil to lymphocyte ratios and increased levels of fibrin were observed in liver biopsies of COVID-19 patients as well as a dilation of portal vein branches, fibrin microthrombi, luminal thrombosis and hepatocyte necrosis[41].

1.8 Coagulation and Fibrinolytic System

In mammals blood gets pumped through a closed circuit, supplies the body with oxygen and is responsible for immune surveillance. In case of a vascular injury, blood starts leaking, platelets and fibrin form clots to seal the leak, preventing excessive bleeding, which is called homeostasis. [42]. Not only due to physical injuries but also in response to infections by different pathogens like bacteria and viruses the coagulation system gets activated. The response helps to limit the spread of pathogens. Therefore, coagulation, immune cells and platelets work together during an infection[42, 43].

If an infection occurs, the blood coagulation system gets activated and immune response and immune system modulations directly interact with components of the hemostatic system[43]. Hemostasis is the response to vascular injury which prevents bleeding and maintains vascular integrity. There are two mechanisms involved in hemostasis which is on one hand the initiation of blood coagulation and on the other hand the activation of platelets[42].

Blood coagulation happens as blood gets exposed to the transmembrane protein tissue factor (TF). Normally TF is not expressed by cells like circulating blood cells or endothelial cells[43]. TF is a membrane bound glycoprotein on vessel walls that is not exposed to blood[42]. Subendothelial cells like pericytes, fibroblasts and smooth muscle cells express high levels of TF. Upon injury, the sudden exposure of TF to the blood stream leads to a direct activation of the coagulation cascade[43].

As the coagulation gets activated leukocytes are recruited and clot components like fibrin serve as a scaffold for the adherence and migration of cells. Leukocytes enhance coagulation as they express TF and they release TF and microvesicles. Moreover, leukocytes are important in the cross-communication between blood coagulation and the immune response. Neutrophils release NETs which also have coagulation enhancing activity. Fibrin(ogen) is important in hemostasis and thrombosis and fibrin clots induce proinflammatory responses. TF expressed by monocytes and macrophages is the primary source leading to inflammation and aberrant coagulation[43].

With the initiation of the coagulation cascade platelet activity is primarily associated. The first step in primary hemostasis is the adhesion of platelets to the extracellular matrix[44]. Platelets get activated due to contact with subendothelial matrix proteins like collagen, fibronectin or von Willebrand factor[45]. Von Willebrand factor for example forms a connection between exposed collagen and a platelet glycoprotein receptor complex on the platelet membrane under

conditions of high shear. Collagen can bind directly to platelet glycoprotein receptors[44]. The activation of platelets leads to exposed anionic phospholipids on the surface, which serve as a place for procoagulant protein assembly[45]. Platelets and fibrin, both initiating the hemostatic response, form a clot and seal the leak as fibrin is the main glue-like product. Fibrin is formed by the activation of blood-borne serine proteases and their cofactors. With the help of the proteolytic action thrombin (factor IIa) fibrinogen is converted to fibrin. Thrombin that circulates inactive as prothrombin or factor II is activated within the prothrombinase complex consisting of serine protease activated factor X (FXa) and cofactors activated factor V (FVa). To activate this prothrombinase complex there are two pathways. The intrinsic or contact pathway which requires contact with a negatively charged surface and involves the coagulation factors XII, XI, IX, VIII and V as well as kininogen and kallikrein, or the extrinsic pathway which involves TF exposed to the circulation as well as coagulation factor VII[42]. To control the coagulation and prevent an uncontrolled state there are control mechanisms, natural anticoagulants like the tissue factor pathway inhibitor and antithrombin[42]. The whole coagulation cascade can be seen in Fig.2.

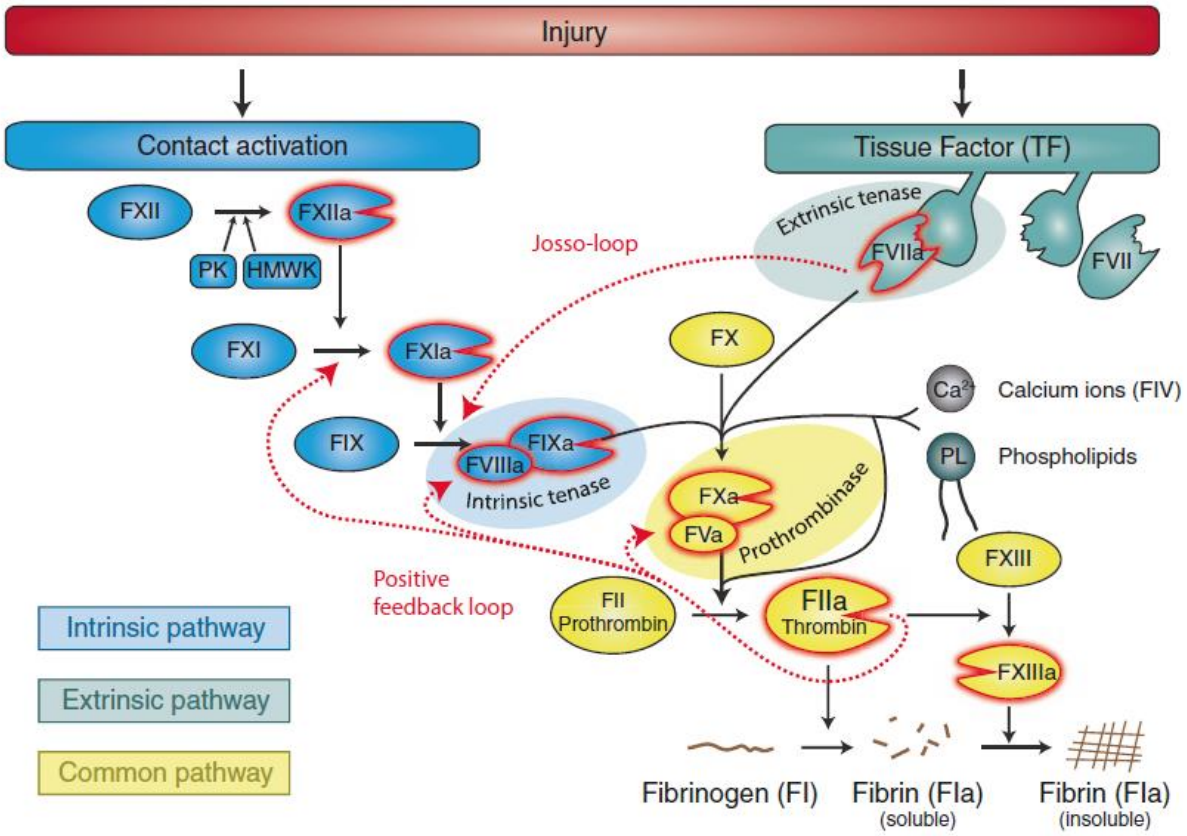

Figure 2: Overview of the coagulation cascade. The cascade can be divided into 3 parts: the intrinsic, extrinsic and common pathway. The intrinsic pathway is activated by contact whereas the extrinsic is activated by tissue factor (TF). The common pathway is activated by FX coming from either intrinsic or extrinsic pathway. Figure is taken from Fundamentals of Vascular Biology (Fig.8.3).[46]

Coagulation as well as fibrinolysis are regulated by substrates, activators, inhibitors, receptors and cofactors. Fibrinolysis is the process of degrading fibrin which was first generated in the coagulation cascade where fibrinogen was converted to fibrin by platelet activation to generate thrombin[47].

The major protease in the fibrinolytic system is plasmin. Plasminogen (PLG) which is a circulating plasma zymogen, that is primarily synthesized in the liver, is cleaved by tissue PLG activator (tPA) and urokinase PLG activator (uPA) to form plasmin. Due to a positive feedback loop, plasmin cleaves tPA and uPA which transforms them from single chain to a more active two chain polypeptide, therefore enhancing its own cleavage and activation. Some cell types like neutrophils, macrophages, monocytes and endothelial cells promote plasmin generation as PLG, and uPA are bound and work as cell surface receptors[47]. uPA is produced by

macrophages, monocytes and urinary epithelium whereas tPA is produced by endothelial cells[45].

The major plasmin substrate fibrin regulates its own degradation by binding PLG and tPA on its surface, which enhances plasmin generation. Fibrin degradation can also be regulated by inhibitors like PLG activator inhibitor-1 (PAI-1) or by inhibitors of plasmin itself like α2-antiplasmin inhibitor[47].

To sum it up, uPA and tPA are enzymes converting PLG to plasmin, plasmin degrades fibrin. PAI-1 is the major uPA and tPA inhibitor, which is pro-thrombotic as PLG cannot be converted to plasmin if uPA or tPA are blocked. This cascade can be seen in Fig.3.

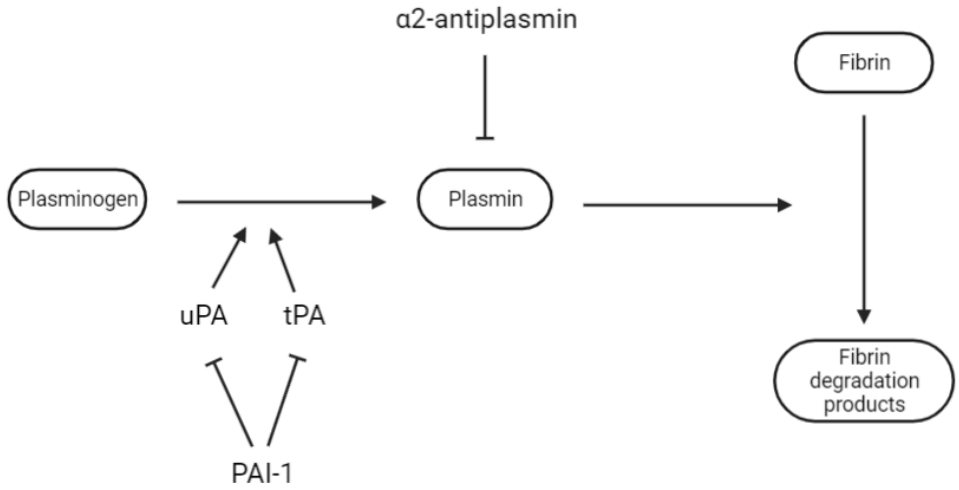

Figure 3: Fibrinolysis pathway. Plasminogen gets converted to Plasmin by the enzymes uPA and tPA which further leads to Fibrin being degraded. Created with BioRender.

1.9 Body Temperature

For many years it is known that the body temperature is a natural indicator of wellbeing, health or illness. In normal physiological conditions, animals are able to contain a steady body temperature independent from the surrounding temperature. In research, especially working with animal models, monitoring the body temperature of the animal is a standard procedure like measuring the weight. Over the years there were several different methods for measuring the body temperature for example the rectal thermometer or thermal microchips. The standardized method is the rectal thermometer, but it has several disadvantages like the stress level of the mouse as it has to be removed from the cage and held by the investigator. Moreover, feces can be a problem and it can be harmful or even not possible considering rectal diseases[48-50].

Another method would be Infrared Thermography (IRT) which is a non-invasive method monitoring physiological and metabolic status and diseases. This was already tested in several species[51, 52]. Products for thermal imaging are commercially available and gained a lot of attention in the biomedical field[53]. IRT functions by measuring the outer body temperature in distance, without contact or stress for the animals[51]. This technology is not only used for outer body temperature but there are different cameras and methods where, among others, the local blood flow can be measured and abnormalities in the blood flow, inflammation or even angiogenesis can be detected[48, 54].

1.10 Microbiome

The mammalian gastrointestinal (GI) microbiota consists of trillions of diverse and complex bacteria and is composed of about 1,000-5,000 species, that equips the host with several health benefits like nutrient digestion, maturation of the mucosal immune system, vitamin synthesis and resistance mechanisms against pathogens. Changes in the GI microbiota are associated with several diseases like metabolic syndrome, colorectal cancer, type two diabetes, atherosclerosis, obesity or chronic inflammation of the GI tract[55, 56]. Studies show the critical role of bacteria and their products concerning homeostasis, function of the innate and adaptive immune system and regulating the development[56].

The altered Schaedler flora (ASF) microbiota, developed by Russell W. Schaedler in 1965, is a defined mouse microbiota colony originally consisting of six bacterial strains isolated from Nelson Collins Swiss mice. The original ASF was refined 1978 by Schaedler´s student Roger P. Orcutt, now consisting of eight microorganisms, which can be seen in Table 1, and eliminated problems which suppliers had with the original one. The ASF offers the opportunity to study a defined host-and-microbe relationship and genome sequencing showed, that the eight selected members have the genetic composition of an entire gut microbiome[55, 57]. As the ASF is closely linked to the host health, modulation of the microbiome shows promising therapeutic potential. If the ASF is well understood it is an experimentally traceable (surrogate) and can be monitored as well as changed[58].

Table 1: The eight members of the altered Schaedler flora (ASF)

ASF #	BACTERIAL SPECIES
ASF 356	*Clostridium species*
ASF 360	*Lactobacillus intestinalis*
ASF 361	*Lactobacillus murinus*
ASF 457	*Mucispirillum schaedleri*
ASF 492	*Eubacterium plexicaudatum*
ASF 500	*Pseudoflavonifractor species*
ASF 502	*Clostridium species*
ASF 519	*Parabacteroides goldsteinii*

2 Aim

The aim of this master thesis was to investigate the host-pathogen interaction during a coronavirus infection. To investigate the inflammatory and prothrombotic modulations during a virus infection in mice, especially in the liver and the lung, we specifically observed several inflammatory markers and coagulation factors. To observe if a virus infection leads to thermoregulatory changes, we measured and observed the body temperature of infected and healthy mice. Further, we aimed to determine, if outer body temperature is a better indicator than body weight regarding the wellbeing of the animals. Finally, we compared coronavirus induced changes in the microbiome, specifically the altered Schaedler's flora to investigate if the coronavirus leads to differences in the gut microbiome.

3 Methods

3.1 qPCR virus burden lung and liver

3.1.1 RNA isolation

To determine the virus burden in lung and liver, small parts of the organs were cut off, 200µl of homogenization buffer (Promega, USA) and a metal bead were added and the samples were shaken for 2 minutes, 30 times per second in the Mixer Mill MM200 (Retsch, Germany). Afterwards 200 µl Lysis Buffer (Promega, USA) were added and the RNA isolation was done automated with the Maxwell RSC simplyRNA Tissue Kit (Promega, USA) with 30 µl RNase and RNA was stored at -80 °C.

3.1.2 cDNA

To convert RNA to cDNA, 10 µl of the liver RNA were taken and mixed with 2 µl GoScript enzyme-mix (Novus, USA) and 8 µl GoTaq Master mix (Novus, USA) consisting of 4 µl nuclease free water, 4 µl GoSkript reaction buffer (random primer) and 2 µl GoSkript enzyme-mix. The samples were put into a 96-well plate (BIO-RAD, USA) and cDNA was produced in the Biometra TOne Thermocycler (Analytik-Jena, Germany) with a program of 25 °C for 5 minutes, 42 °C for one hour and 70 °C for twelve minutes.

3.1.3 qPCR

qPCR Mastermix was done as seen in Table 2. 6 µl Mastermix were added to 1 µl cDNA per sample. The targets can be found in Table 3. The corresponding probe from the Universal Probe Library Set (Roche, Switzerland) and the GoTaq Probe qPCR MasterMix (Promega, USA) was used. The qPCR was run on a Thermal Cycler (BIO-RAD, USA) with the protocol seen in Table 4. For analysis the fold difference was calculated and statistics were done with GrapPad Prism 8.

Table 2: qPCR Mastermix for virus burden in lung and liver.

0.014µl	Forward Primer
0.014µl	Reverse Primer
0.07µl	UPL Probe
3.5µl	GoTaq Probe qPCR MasterMix, 2x (Promega, USA)
2.4µl	Nuclease free water

Table 3: qPCR Targets for virus burden in lung and liver.

Target	Forward Primer (5´-3´)	Reverse Primer (3´-5´)	Probe
β-actin	ctaaggccaaccgtgaaaag	accagaggcatacagggaca	64
PolyU	tgtgtgagagaagttagcaagg	gcaggaatagtaccctgatgtg	56-FAM/TGGAGTATG/ZEN/ GAACGGCGATAGGCGC/ 3IAKkFQ
Nsp12	agggagtttgaccttgttcag	ataatgcacctgtcatcctcg	56-FAM/TGGAGTATG/ZEN/ ACCTACCACCCGAACAC/ 3IABkFQ

Table 4: qPCR protocol for virus burden in lung and liver.

Time	**Temperature**	
10min	95°C	
10s	95°C	
20s	60°C	49x
6s + reading plate	72°C	
10min	25°C	

3.2 Immunohistochemistry - CitH4 staining lung and liver

Freshly isolated lung and liver tissue was fixed with 4 % formaldehyde, embedded in paraffin and cut in 5 µm thick slices.

Paraffin embedded tissue was deparaffinized with xylol 1 (Fisher Chemical, USA) (3 min), xylol 2 (Fisher Chemical, USA) (6 min), 100 % EtOH (3min), 95 % EtOH (3 min), 85 % EtOH (3 min), 70 % EtOH (3 min), 1x PBS (PBS-Buffer pH 7.4, Morphisto, Austria) (3 min). Then autoclaved (CertoClavl, Austria) at 120 °C in 1x Dako target retrieval solution (Dako, USA) for target retrieval.

For fluorescence staining blocking was done with blocking buffer (2 % BSA, 0.5 % Fish Gelatin, 0.3 % Tween20, in PBS (Sigmal-Aldrich, USA/Morphisto, Austria)) for 1.5 hours at room temperature. Samples were washed three times in 1x PBS. As primary antibodies 100 µl of Histone H4 (CitH4, Millipore-Merk, USA, 1:100, rabbit) and MPO (R&D, USA, goat, 1:66) were used and incubated at 4 °C over night. As secondary antibody for CitH4 100 µl of DyLight550 rabbit (0.5 mg/ml, Invitrogen, USA) and for MPO 100 µl of DyLight650 goat (0.5 mg/ml, Abcam, US) were used and incubated for two hours at room temperature. Samples were washed 3x in 1xPBS and incubated with DAPI (1:2000) for 30 minutes. Afterward the

tissue was 3x washed in 1x PBS and mounted with mountant permafluor media (Epredia, USA), covered with a cover slide and stored at 4 °C.

3.2.1 Scanning of CitH4 stained slides and analysis

The finished CitH4 stained tissues was scanned with the Zeiss Observer.Z1 fluorescents Microscope (Zeiss, Germany) with the digital camera orca-flash4.0 (Hamamatsu, Germany) and the fluorescence lamp X-Cite 120PCQ (Lumen Dynamics, Canada). Settings were set in TissueFAXS 7.131 scanning software (TissueGnostics, Austria) using different channels for DyLight650, DyLight550 and DAPI. Pictures where then exported from TissueFAXS Viewer, opened in ImageJ and thrombi were counted. Area of the tissue was measured with ImageJ and divided by counted thrombi to receive thrombi per area tissue.

3.3 qPCR inflammatory markers and PAI, PLG, uPA

The same cDNA as already described in 2.1.1 was taken and qPCR Mastermix was done as seen in Table 5. 6 µl Mastermix were added to 1 µl cDNA per sample. The targets can be found in Table 6. The corresponding probe from the Universal Probe Library Set (Roche, Switzerland) or self-designed and ordered from IDT (Integrated DNA Technologies, Belgium) as well as the GoTaq Probe qPCR MasterMix (Promega, USA) was used. The qPCR was run in the Thermal Cycler (BIO-RAD, USA) with the protocol seen in Table 7. For analysis the fold difference was calculated and statistics were done with GrapPad Prism 8.

Table 5:qPCR Mastermix for inflammation, PAI, PLG and uPA.

0.014µl	Forward Primer
0.014µl	Reverse Primer
0.07µl	UPL Probe
3.5µl	GoTaq Probe qPCR MasterMix, 2x (Promega, USA)
2.4µl	Nuclease free water

Table 6: qPCR Targets for inflammation, PAI, PLG and uPA.

Target	Forward Primer (5′-3′)	Reverse Primer (3′-5′)	UPL Probe
GAPDH	gtcggtgtgaacggattt	ggaacatgtagacatgtagtt	9
ICAM-1	cccacgctacctctgctc	gatggatacctgagcatcacc	81
IFNα	tcaagccatccttgtgctaa	gtcttttgatgtgaagaggttcaa	3
P-selectin	gagggaagaaagccagacg	ggcgtccaggaacctttt	71
TNFα	ctgtagcccacgtcgtagc	ttgagatccatgccgttg	25
VCAM-1	gagaatgaacactcttacctgtgc	tggatccttggggaaagagt	21
IFIT-1	tgaaatgccaagtagcaaggt	cctgctagacagggtcagaaa	2
IFIT-2	caatgcttaggggaagctga	tgatttctacttggtcaggatgc	42
IFNβ-1	ctggcttccatcatgaacaa	agagggctgtggtggagaa	18
IFNγ	atctggaggaactggcaaaa	ttcaagacttcaaagagtctgaggta	21
Ly6G	cctgtgtgctcatccttctt	tagttgtgttgcaggaagtctc	56-FAM/ACTGTGTGC/ZEN/AGAAAGAGCTCAGGG/3IABkFQ
PAI-1	aggatcgaggtaaacgagagc	gcgggctgagatgacaaa	69
PLG	gcatcaccagaccagtcaga	tggtagcattcctggaccac	31
uPA	ggagcagctcatcttgcac	cccgtgctggtacgtatctt	64

Table 7: qPCR protocol for inflammation, PAI, PLG and uPA.

Time	**Temperature**	
10min	95°C	
10s	95°C	
20s	60°C	49x
6s + reading plate	72°C	
10min	25°C	

3.4 Organ culture

3.4.1 Culturing liver

Liver was extracted from C57Bl/6 mice, cut in small pieces and equally distributed into 48-well plate (Greiner bio-one, Austria) as it can be seen in Fig.4. Five liver pieces were taken per condition. The stock TNFα (100 ng/µl), IL-4 (200 µg/ml), INFγ (1.42 mg/ml) were diluted to 25 ng/ml and 50 ng/ml and 100 ng/ml in RPMI-1640 Medium (Sigma-Aldrich, USA) with 10% FBS (FBS Gold special processed, Seraglob, Switzerland) and PSFG (Antibiotic mix, Penicillin, Streptomycin, Fungizone, Glutamine, Lonza, Switzerland). 250 µl Medium were used per well and the liver was incubated for six hours. The RNA was extracted with the Maxwell RSC simplyRNA Tissue (Promega, USA) with 30 µl RNase and stored at -80 °C.

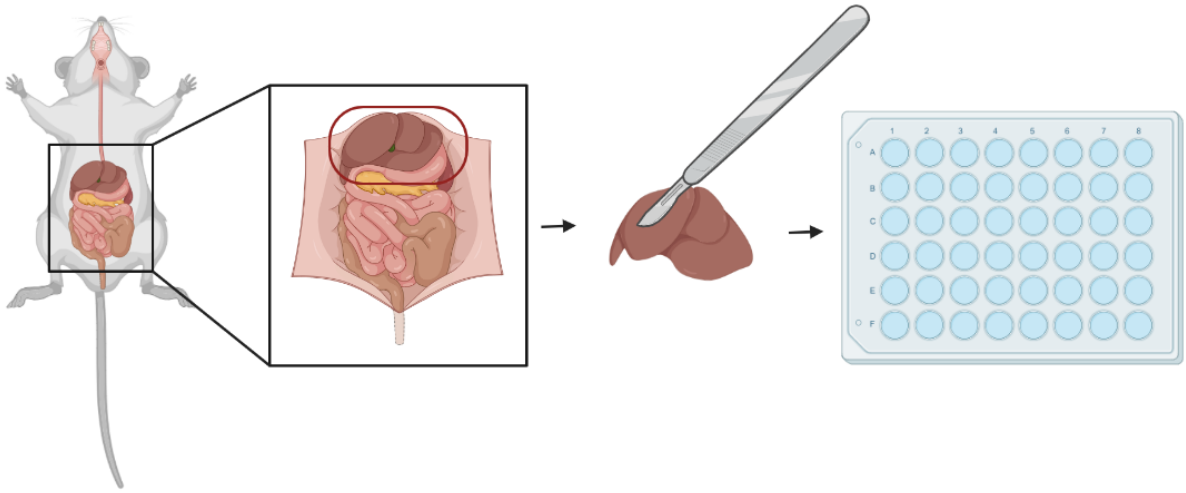

Figure 4: Experimental setup of the organ culture. Liver from Bl6 mice were taken, cut in small pieces and incubated for 6h in different conditions. Created with BioRender.

3.4.2 cDNA

Done as already described in 3.1.2.

3.4.3 qPCR

To quantify the cDNA a qPCR was done with a Mastermix as it can be seen in Table 8. The targets can be found in Table 9. The corresponding Probe form the Universal Probe Library Set (Roche, Switzerland) and the GoTaq Probe qPCR MasterMix (Promega, USA) was used. 1 µl of cDNA was mixed with 6 µl of the qPCR Mastermix. The qPCR was run in the Thermal Cycler (BIO-RAD, USA) with the protocol seen in Table 10. For analysis the fold difference was calculated and statistics were done with GrapPad Prism 8.

Table 8: qPCR Mastermix for organ culture samples.

0.014µl	Forward Primer
0.014µl	Reverse Primer
0.07µl	UPL Probe
3.5µl	GoTaq Probe qPCR MasterMix, 2x (Promega, USA)
2.4µl	Nuclease free water

Table 9: qPCR targets for organ culture samples.

Target	Forward Primer (5´-3´)	Reverse Primer (3´-5´)	Probe
18S	cacggacaggattgacagatt	gccagagtctcgttcgttatc	40
PAI-1	aggatcgaggtaaacgagagc	gcgggctgagatgacaaa	69
PLG	gcatcaccagaccagtcaga	tggtagcattcctggaccac	31
uPA	ggagcagctcatcttgcac	cccgtgctggtacgtatctt	64
TGFβ-1	tggagcaacatgtggaactc	gtcagcagccggttacca	2

Table 10: qPCR protocol for organ culture samples.

Time	**Temperature**	
10min	95°C	
10s	95°C	49x
20s	60°C	
6s + reading plate	72°C	
10min	25°C	

3.5 Trichrome staining collagen

For the trichome staining the kit from Sigma-Aldrich, USA, as well as their standard protocol was used. The slides were deparaffinized as already described in 2.2. and put in deionized water. Samples were put in Bouin´s Solution at 56 °C for 15 minutes. Slides were cooled in tap water and washed till the yellow color was removed. Slides were put in Working Weigert´s Iron Hematoxylin Solution for 5 minutes and afterwards washed with tab water for 5 minutes. They were rinsed with deionized water and stained in Biebrich Scarlet-Acid Fuchsin for 5 minutes. Afterwards again rinsed with deionized water. Next, they were put in Working Phosphotungstic/Phosphomolybdic Acid Solution for 5 minutes, then in Aniline Blue Solution for 5 minutes and then in 1 % Acetic Acid for 2 minutes. The slides were then dehydrated with alcohol, 70 %, 85 %, 95 % and 100 % EtOH and then cleared in Xylol (Fisher Chemicals, USA) and mounted with mountant permafluor media (Epredia, USA), covered with a cover slide and stored at room temperature.

3.5.1 Scanning of Trichrome stained slides and analysis

Trichrome slides were scanned with the Grundium Ocus40 Microscope scanner MGU-00004 (Grundium, Finland) with an Olympus UPlanXApo 20x/0.80 Lens. Pictures were saved as svs., exported to OlyVIA software, saved as tif. and thrombi were counted in ImageJ. Area of the

tissue was measured with ImageJ and divided by counted thrombi to receive thrombi per area tissue.

3.6 Flow cytometry for low dose infection

3.6.1 Lung preparation

For flow cytometry the right superior and inferior lobe of the lung were taken, cut in tiny pieces and incubated for 60 minutes in 3 ml HBSS supplemented with 2 mg/ml collagenase IV with 50 U/ml DNase I (400 U/ml, 6.25 mg/50 ml) at 37 °C shaking. Resulting lung cells were filtered through a 70 µm cell strainer and washed with 7 ml 1xPBS. Samples were centrifuged at 500xg for 7 minutes at 4 °C and the supernatant was discarded. 1 ml erylysis buffer was added and incubated for 3-5 minutes. Erylysis was stopped with 9 ml 1xPBS. Samples were centrifuged at 500 x g for 7 min at 4 °C and supernatant was removed. Lung was resuspended in 200 µl 1xPBS and kept on ice till flow cytometry.

3.6.2 Flow cytometry

5 µl of lung tissue cells were stained with 5 µl of antibodies for 15 minutes. 190 ml of 1xPBS were added and centrifuged for 5 minutes with 500 x g. The supernatant was removed and sample were resuspended in 150 µl 1 % PFA. The flow cytometry targets can be seen in Table 11 for the T-cells and in Table 12 for the monocytes and macrophages. Cells were measured with an Attune NxT flow cytometer and data analyzed with Attune NxT Software v3.1.2.

Table 11: T-cell mix for flow cytometry.

Target	**Clone**	**Conjugate**	**µl/sample**
CD3	17A2	APC/Cy7	0.1
CD4	RM4-5	PerCP	0.1
CD8	53-6.7	BV605	0.2
CD25	3C7	PE/Cy7	0.1
CD44	IM7	PE	0.1
CD62L	MEL-14	APC	0.1
CCR7 (CD197)	4B12	BV421	0.4
PBS			3.9

Table 12: Monocytes and macrophages mix for flow cytometry.

Target	Clone	Conjugate	µl/sample
CD11b	M1/70	PE/Cy7	0.05
CD45	30-F11	APC/Cy7	0.1
CD64	X54-5/7.1	BV605	0.1
CD115	AFS98	BV421	0.1
CD170 (SiglecF)	S17007L	APC	0.1
Ly6C	HK1.4	PE	0.05
PBS			4.5

3.7 Temperature measurement with an infrared camera

For measuring the outer body temperature mice were placed in single cages with a nonreflective plastic floorplate. Two mice were measure simultaneously which can be seen in Fig.5. The commercially available FLIR infrared camera (FLIR T860 with FLIR wide angle lens f=10mm) was placed above the cage, the cage was covered with plastic wrap and infrared pictures were taken every 10 seconds for 2 minutes acquiring twelve images. Settings were put to temp -20 to 120, autofocus off. Pictures were analyzed with ResearchIR (64-bit) where the best 5-7 pictures were selected and the mean body temperature was measured. Statistics were done with GraphPad Prism 8. The temperature and humidity in the closed housing system (Tecniplast, Germany) was constantly measured being 23 °C and 49-57 relative humidity.

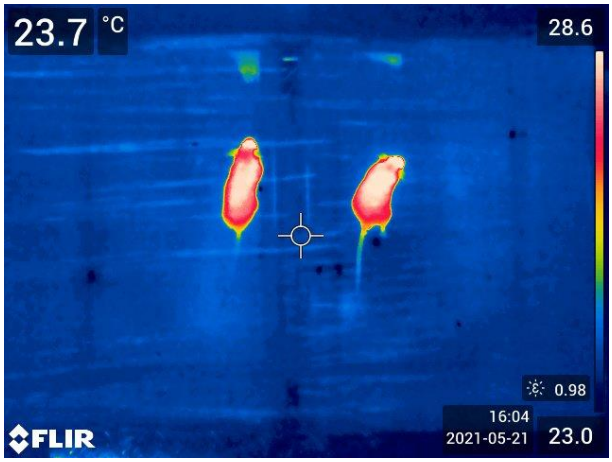

Figure 5: FLIR temperature picture showing 2 mice which can be measured simultaneously in 2 separate cages.

3.8 Microbiome analysis of the Altered Schaedler Flora

For the fecal DNA extraction Maxwell RSC Fecal Microbiome Kit (Promega, USA) was used according to their protocol. About 100-300 mg fecal samples were used, homogenized with a metal ball in the Mixer Mill MM200 (Retsch, Germany) for 3 minutes 30 per second. 1 ml of lysis buffer and 40 µl of proteinase K were added, and again homogenized for 3 minutes in the Mixer Mill MM200 (Retsch, Germany). Samples were incubated at 95 °C for 5 minutes, let cooled for 2 minute and vortexed for 1 minute. Samples were incubated at 56 °C for 5 minutes, centrifuged at room temperature for 5 minutes at maximum speed (<10.000 x g), 300 µl liquid were transferred to reagent cartridge. Fecal microbiome protocol was run on Maxwell RSC (Promega, USA).

qPCR targets were designed as published by Gomes-Neto, J. C. at al [55] and ordered from Integrated DNA technologies (IDT, USA) and Eurofins genomics (Luxemburg) and can be seen in Table 13. The mastermix was used as seen in Table 14. The qPCR was run in the Thermal Cycler (BIO-RAD, USA) with the protocol seen in Table 15. For analysis the fold difference was calculated and statistics were done with GrapPad Prism 8.

Table 13: qPCR targets microbiome.

Target	Forward Primer (5′-3′)	Reverse Primer (3′-5′)
16S (8F&515R)	CTC CTA CGG GAG GCA GCA G	TTA CCG CGG CTG CTG GCAC
356	AAA ATA ATT AGG AGC TTG CTT TTA A	TTA GAA GAT GCC TCC TAA GAA CC
360	GGT GAT GAC GCT GGG AAC	AAG CAA TAG CCA TGC AGC
361	GAA CGA AAC TTC TTT ATC ACC	TAG CAT AGC CAC CTT TTA CA
457	TCT CTT CGG GGA TGA TTA AAC	AAC TTT TCC TAT ATA AAC ATG CAC
492	AAT TCC TTC GGG GAG GAA GC	TAA AAC CAT GCG GTT TTA AAA AC
500	ACG GAG GAC CCC TGA AGG	AGC GAT AAA TCT TTG ATG TCC
502	GAG CGA AGC ACT TTT TTA GAA C	TTA CAC CAC CTC AGT TTT TAC C
519	GCA GCA CGA TGT AGC AAT ACA	TTA ACA AAT ATT TCC ATG TGG AAC

Table 14: qPCR Mastermix for microbiome.

0.014µl	Forward Primer
0.014µl	Reverse Primer
3.5µl	GoTaq qPCR Master Mix, 2x (Promega)
2.47µl	Nuclease free water

Table 15: qPCR protocol for microbiome.

Temperature	Time	
95°C	10min	
95°C	15s	
57°C	30s	60x
72°C	30s	
72°C	5min	
25°C	10s	

3.9 qPCR analysis and Graphs

qPCRs were analyzed by calculating the dCT by subtracting the housekeeper gene (18S, 16S, β-actin or GAPDH) from the CT value. Then the 2^-dCT was calculated and the data was transferred to GraphPad Prism 8 for further statistics and visualization. For statistics an unpaired, parametric or nonparametric, depending on the normality distribution, t-test was used. All graphs for all experiments were done with GraphPad Prism 8 as well as all statistics.

4 Results

4.1 Virus infection and NET formation in the lung

C57Bl/6 mice were infected with 1.5*10^6 $TCID_{50}$ and the virus burden in the lung was analyzed with by qPCR. As depictured in Fig.6A the virus concentration was high at day two after the infection and lowers significantly till day ten. As it has been described, that there was a higher NET formation during an infection with the coronavirus, the next step was to investigate the thrombus formation in the lung with the help of a CitH4 staining (Fig.6B). A significant increase of NETs from day two to day four and a further increase at day ten could be observed.

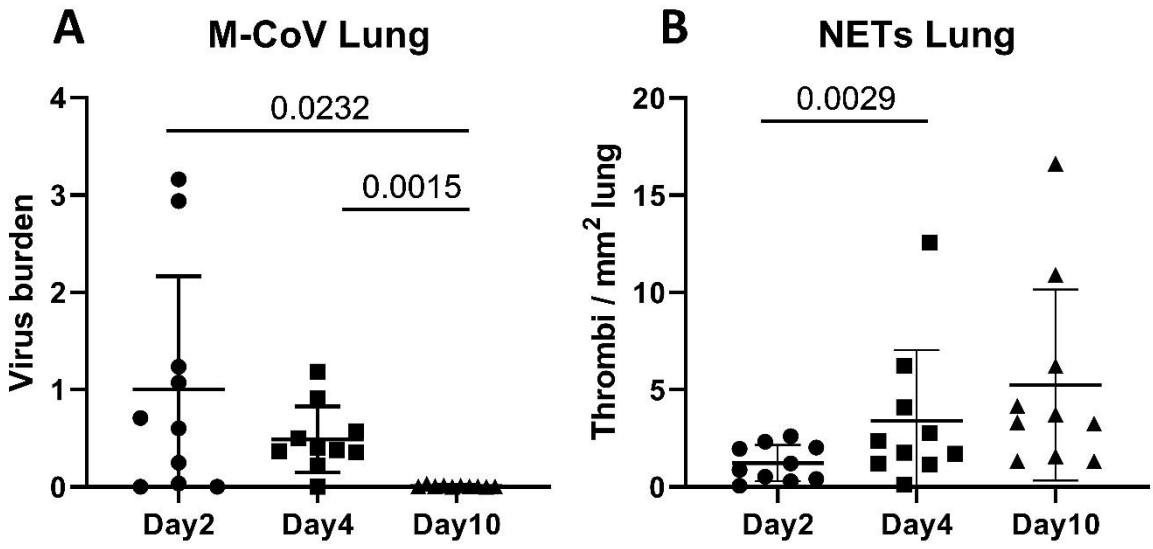

Figure 6: A) qPCR of the virus burden in mice lung at day 2, day 4 and day 10. B) CitH4 staining for NET formation in lung at day 2, day 4 and day 10. Data normalized to day 2. Statistics done with t-test. (n=10, mean+/-stdv)

Fig.7 shows the CitH4 staining, which was done with DAPI staining of the nucleus, MPO staining of the activated neutrophils and CitH4 as a marker for NET formation. Only thrombi that were clearly identified and showed a compact formation were selected.

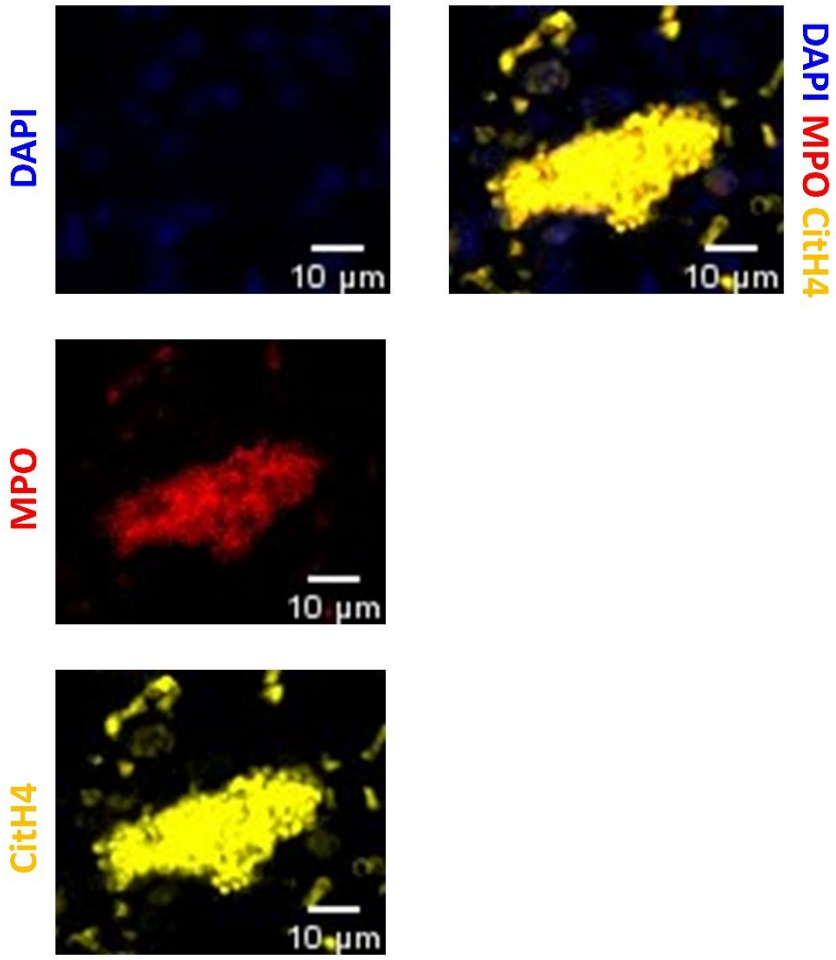

Figure 7: DAPI, MPO and CitH4 staining of a lung thrombus with a merged CitH4 positive thrombus in the mouse lung.

4.2 Virus infection and NET formation in the liver

As a very interesting effect could be observed in the lung, the next step was to study the influence of MCoV in the liver. Different to the lung, the liver showed the highest virus burden on day four (Fig.8A). Additionally, the NET formation was different (Fig.8B), as NETs in the liver can be found already on day two. The number of NETs decreased at day four and increased again at day ten.

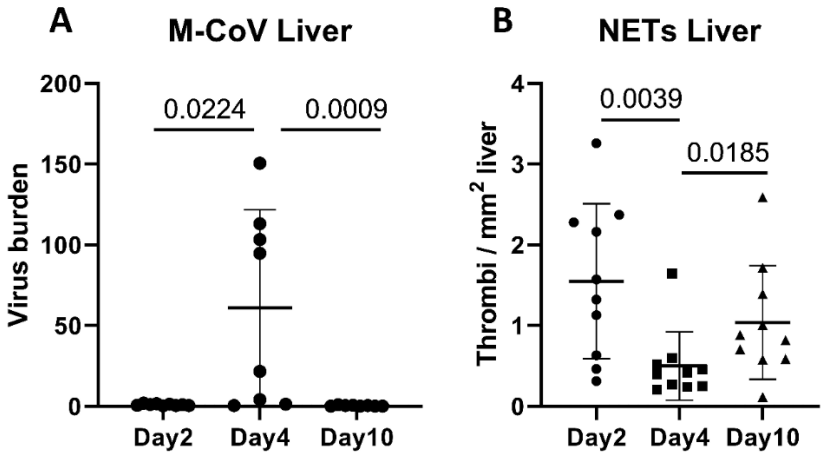

Figure 8: A) Virus burden in mice liver at day 2, day4, day10. B) NET formation in liver at day 2, day 4, day 10. Data normalized to day 2. Statistics done with t-test. (n=10, mean +/- stdv.)

Fig.9 shows the CitH4 staining of the liver. As already seen in the lung, staining was done with DAPI, MPO and CitH4 and only very condensed and clearly positive NETs were counted.

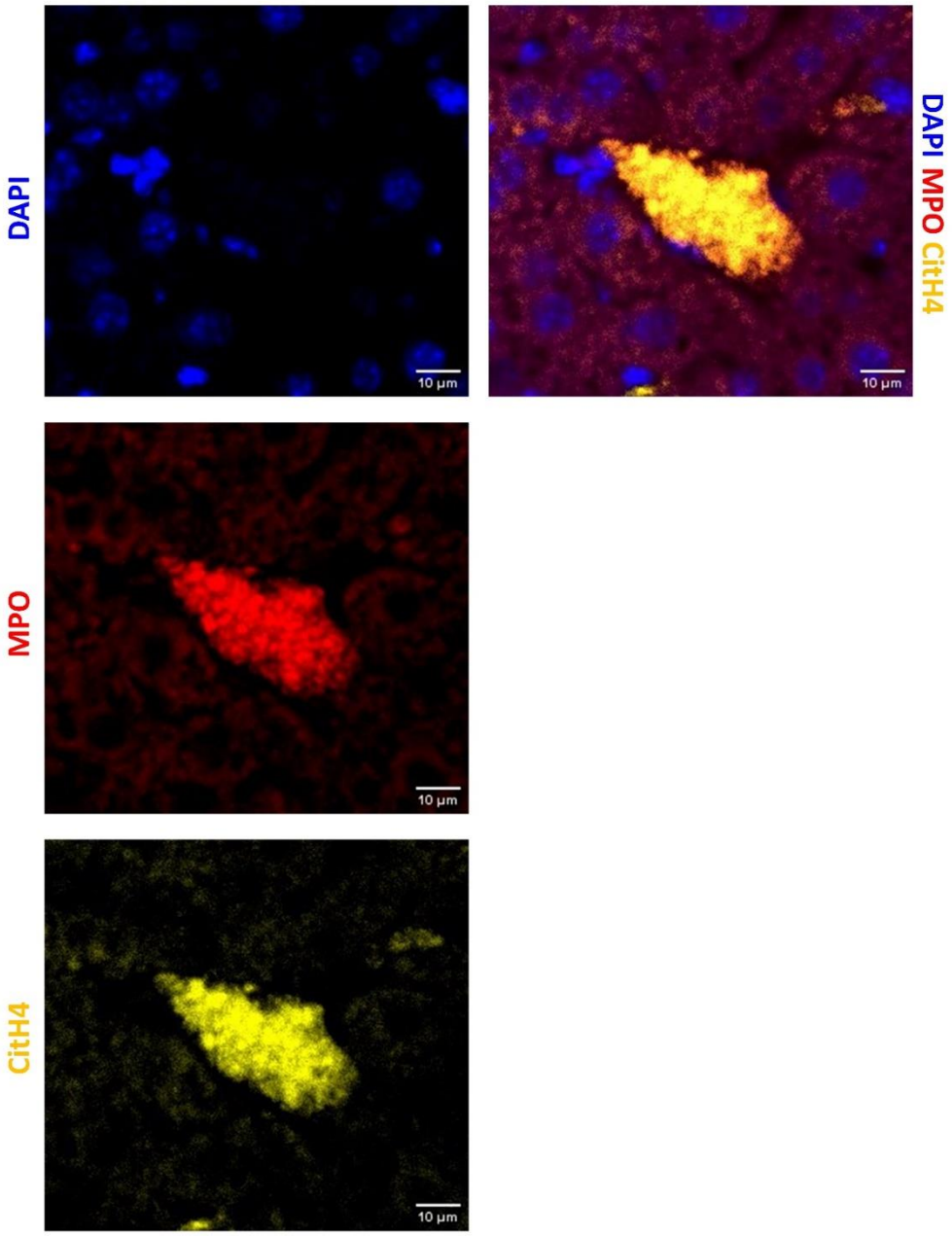

Figure 9: DAPI, MPO and CitH4 staining of a liver thrombus with a merged CitH4 positive thrombus in the mouse liver.

4.3 Inflammation markers in liver

As a different behavior of the virus infection and NET formation in the lung compared to the liver was seen, we focused on the liver with the next step investigating inflammation by qPCR. Fig.10 shows that in general the highest inflammation was seen at day four. ICAM-1, P-selectin, VCAM and Ly6G showed the highest fold change at day four and their level stayed high at day

ten. IFNα, TNFα, IFNβ and IFNγ levels were only high at day 4. IFIT-1 and IFIT-2 levels, two IFN response triggered genes, were high at day two and four.

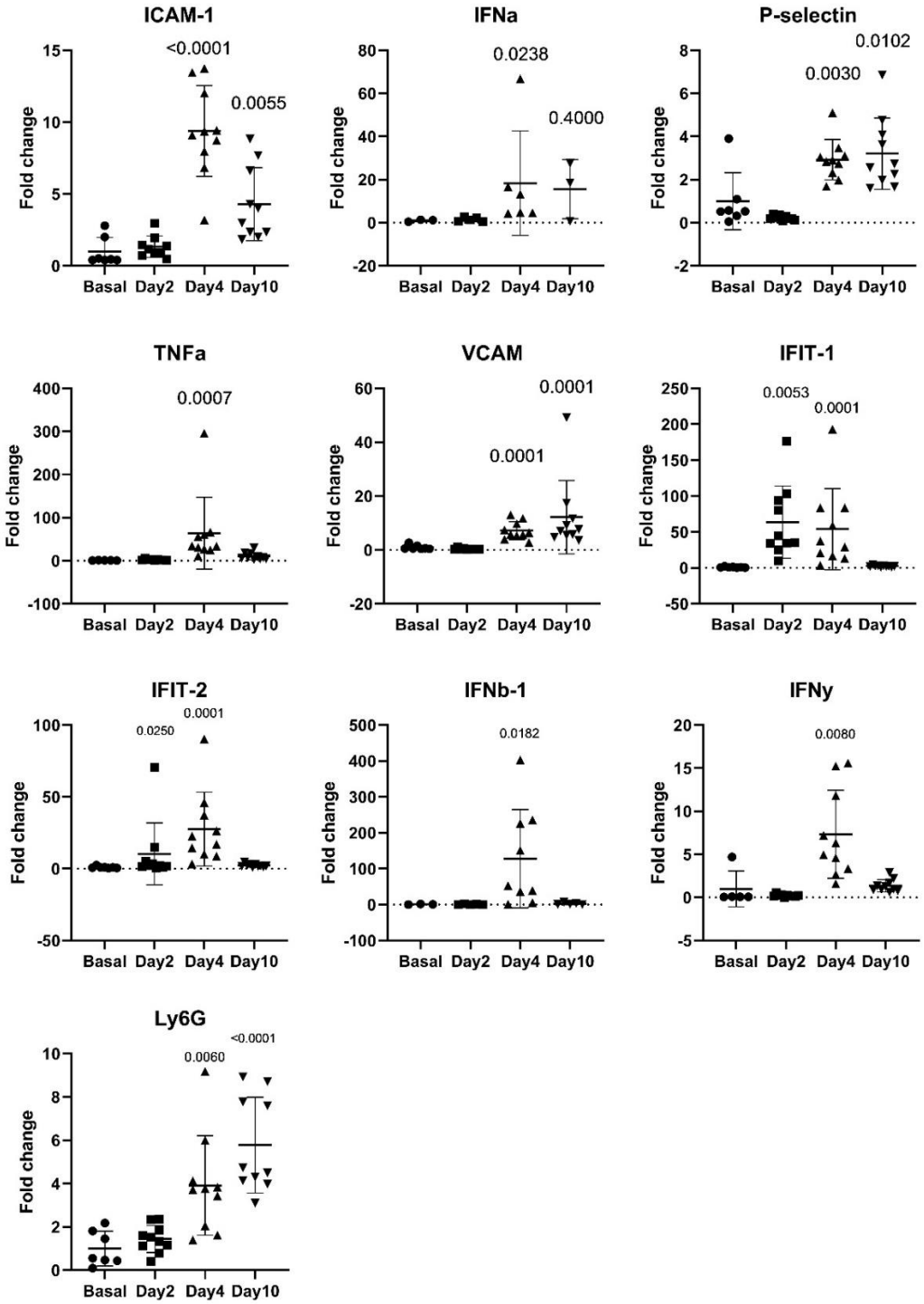

Figure 10: qPCR results of several inflammation markers in the liver. Data is normalized to basal. Statistical analysis was done with a t-test. (n=10, mean+/-stdv.)

4.4 Coagulation and Fibrinolysis

As the NET formation goes hand in hand with coagulation, the next step was to analyze the coagulation targets PAI-1, PLG and uPA by qPCR. Fig.11 shows no significant difference in PLG but changes in PAI-1 and uPA levels. PAI-1 and uPA were significantly increased at day four aligning with the results of the inflammation, where also the highest fold change was observed at day four.

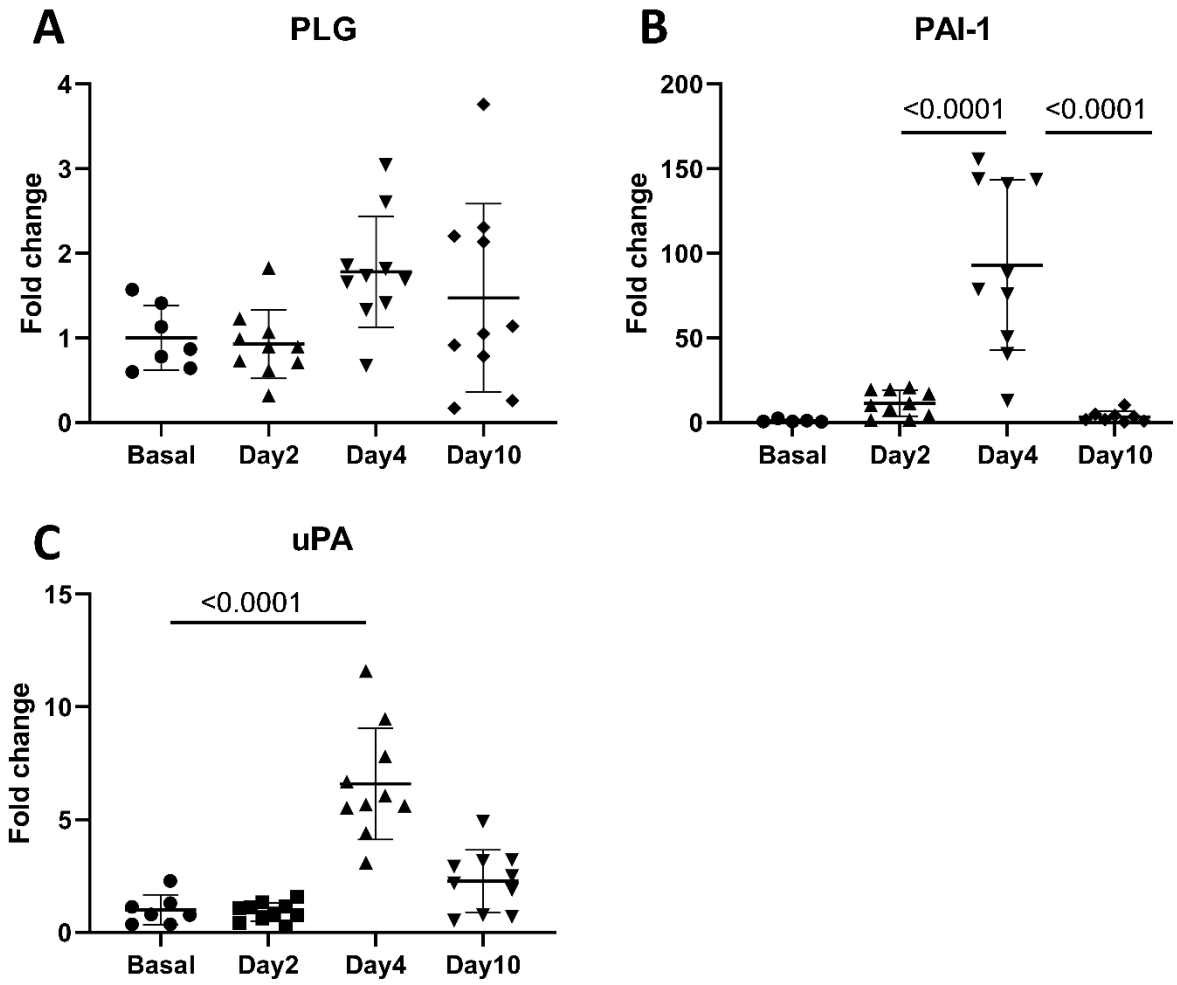

Figure 11: qPCR of PAI-1, PLG and uPA at basal, day 2, day 4, day 10, showing sign. increase at day4 in B and C but no difference in A. (n=10, mean+/-stdv.)

4.5 Organ culture

As the influence of inflammation during an infection with MCoV to PAI-1 and uPA could be observed, the next experiment was to investigate if the same effects can be seen due to increased circulating inflammatory cytokines. We were able to determine that especially TNFα and IFNγ were elevated in the circulation in mice two and four days after virus infection (data not shown).

Therefore, liver from healthy mice was taken and incubated with TNFα (Fig.12A-C), IL-4 (Fig.12D-F) or IFNγ (Fig.12G-I) at three different concentrations and PAI-1, uPA and PLG levels were analyzed. For livers incubated with IFNγ an additional qPCR targeting TGFβ (Fig.12J) was done. In Fig.12A-C we can already observe that incubation with 25 ng/ml TNFα resulted in a significant increase in uPA and PAI expression, whereas there was no difference in PLG. These results align with those of the cytokine profile after virus infection. Similar results can be seen in Fig.12D-I, where in both cases PAI and PLG were not significantly different, but uPA was increased with IL-4 stimulation at the highest concentration of 100 ng/ml and with IFNγ stimulation already at 25 ng/ml. Additional TGFβ was significantly increased in livers stimulated with IFNγ at all concentrations.

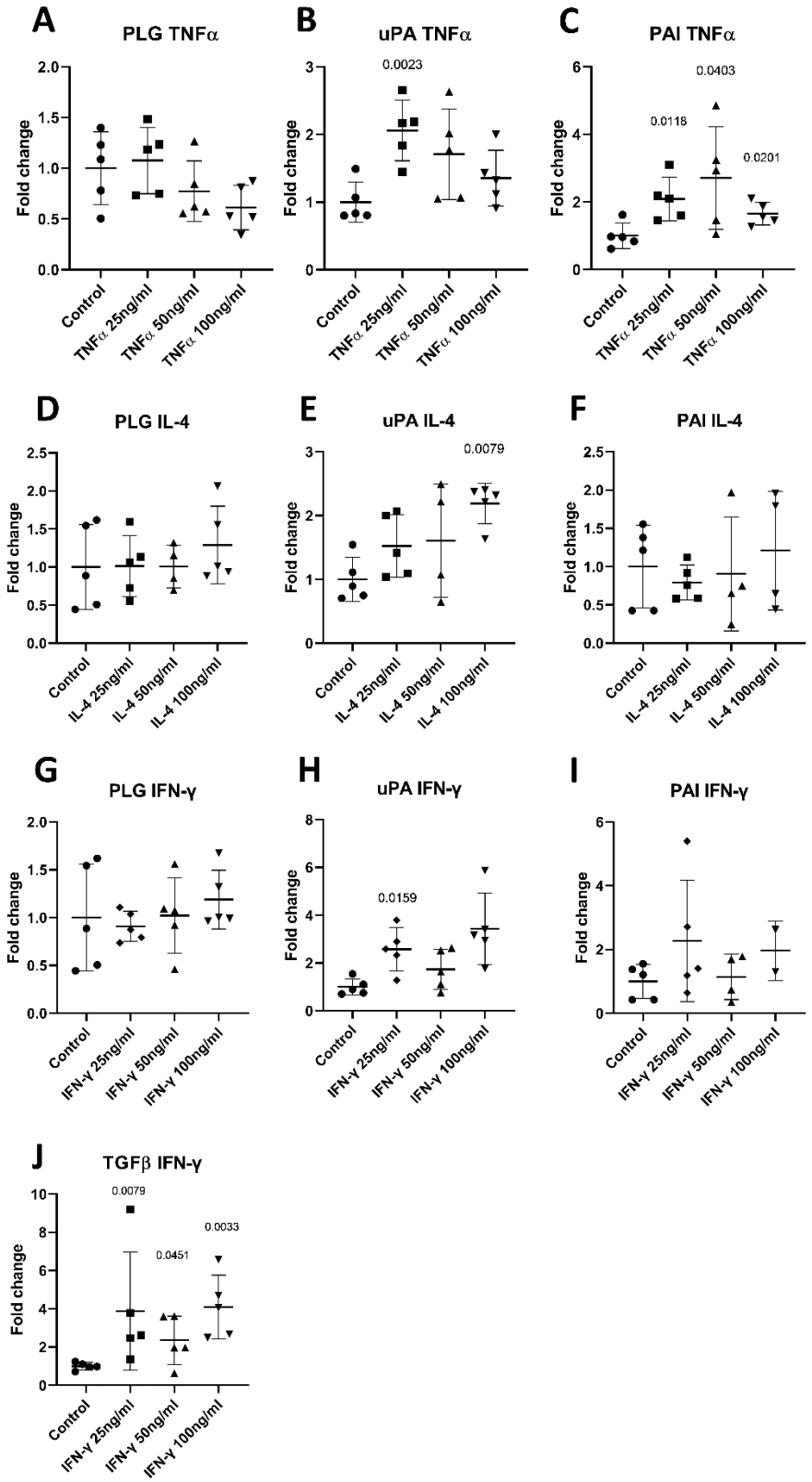

Figure 12: PLG, uPA, PAI and TGFb levels of liver in organ culture for 6h with 3 different concentrations of TNFa, IL4 and IFN-y(n=5, mean+/-stdv.)

4.6 Collagen in Lung and Liver

To determine if different expression and activation profiles in lung and liver would also lead to changed fibrosis behavior, we investigated collagen deposits via immunohistochemistry in both lung and liver (Fig.13A-B). In the lung, as it can be seen in Fig.13A, a decrease in collagen at day two with a significant increase on day four compared to the basal percentage was observed. In the liver, which can be seen in Fig.13B, there is a significant increase in collagen at day ten compared to basal. This result aligns with the prothrombin qPCR results in the liver in Fig.13C which was also significantly higher at day ten.

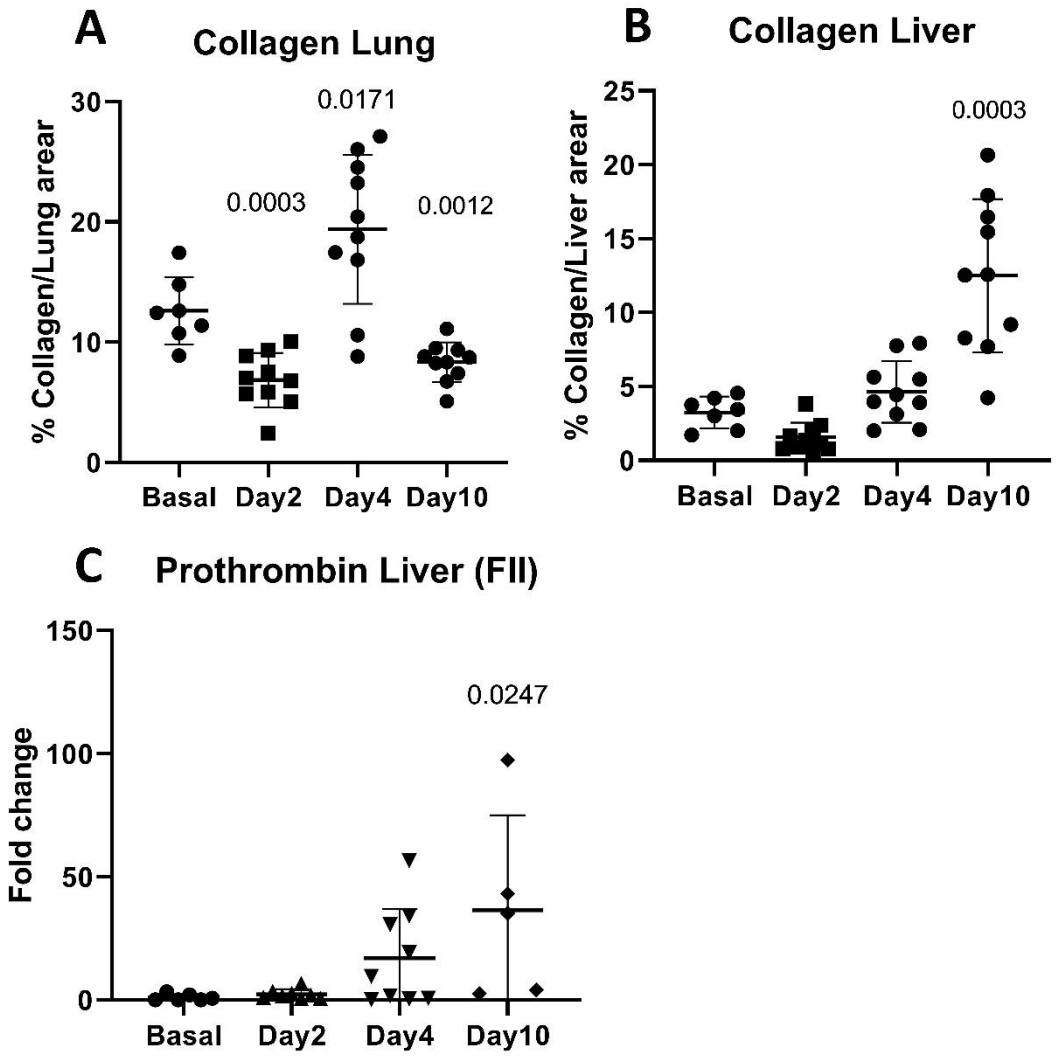

Figure 13:Trichrome staining of collagen in lung and liver and qPCR of prothrombin. (Basal n=7 Day2,4,10 n=10, mean+/-stdv.)

Fig.14 shows a trichrome staining in A the liver and B the lung with collagen in blue. For the analysis the vessels were cut out with the tightly surrounding endothelium and collagen to only measure the collagen that can be found deposited in the tissue.

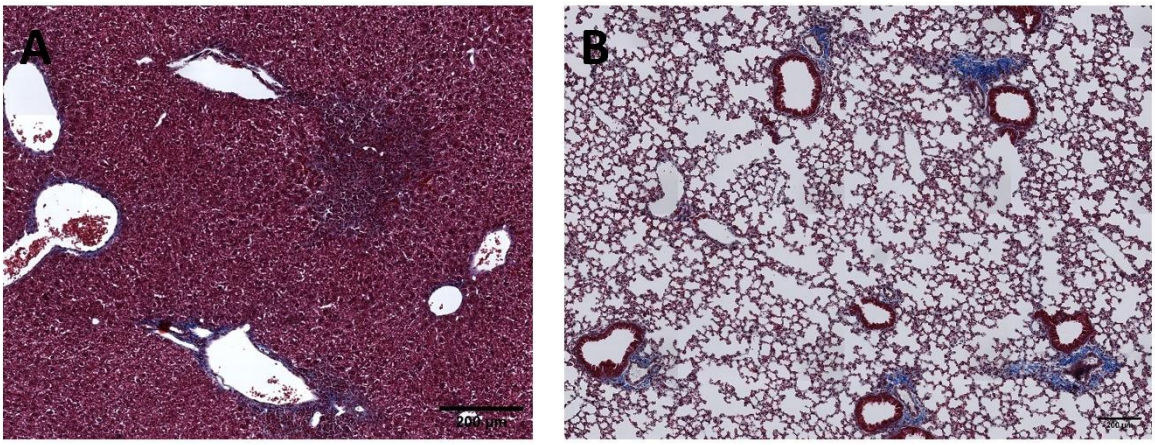

Figure 14: Trichrome staining of A) liver B) lung. Blue indicating collagen.

4.7 Low concentration MCoV infection

For all previous experiments mice were infected with MCoV with a $TCID_{50}$ of 1.5*10^6. For this experiment a $TCID_{50}$ of 1400, a low dose of MCoV, was used. Showing in Fig.15 that even with this low concentration there is a significant increase of CD3+, CD4+ and CD8+ cells at day two in the lung. Also, lung memory and naïve T-cells were significantly higher at day two and effector T-cells were lower. Moreover, intestinal and alveolar macrophages were significantly high at day two. Special about these results is that the $TCID_{50}$ was so low, that there was no detectable virus burden left at day 2 but still an inflammation and immune reaction.

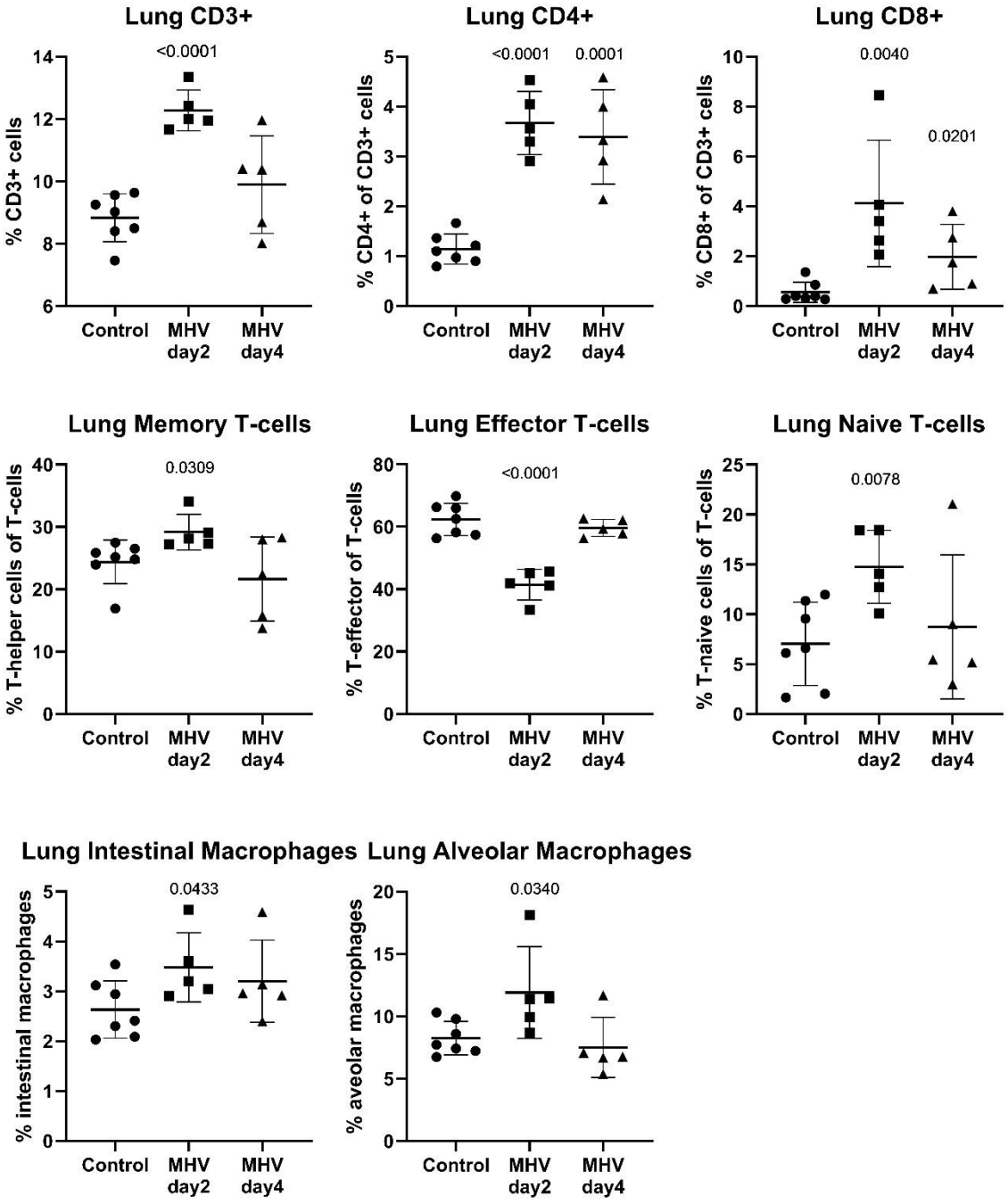

Figure 15: Low concentration M-CoV infection in the lung showing B-cells, T-cells and macrophages. (n=7 control, n=5 MHV, mean+/-stdv.)

4.8 Comparing temperature to weight loss during a MCoV infection

The temperature was measured as already described with the FLIR infrared camera twice a day as well as the weight was measured at the same timepoints during an MCoV infection with a $TCID_{50}$ of 1.5*10^6. Looking at the grouped temperature and weight, which can be seen in

Fig.16, a loss of temperature can be observed over the ten days. Mouse 306 (male) had a significant weight loss close to the termination criteria of 20% weight loss but holding a steady temperature as well as mouse 301 (female). Mouse 308 (female) lost weight as well as temperature from day five on and had to be sacrificed at day seven. A simultaneous loss of temperature as well as weight can be observed.

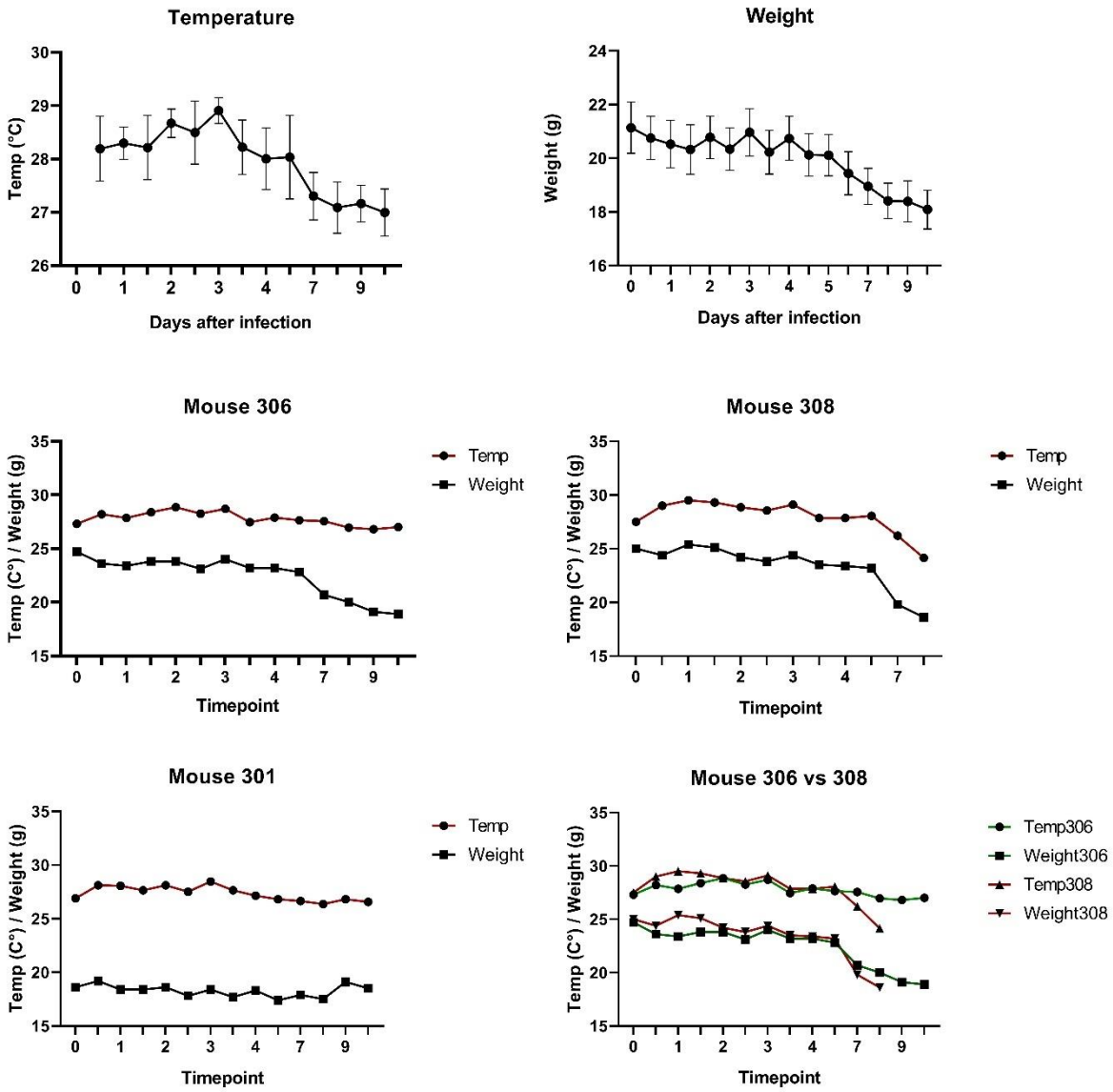

Figure 16: Grouped temperature and weight measured AM and PM for ten days. Mouse 306 and 301 survived, mouse 308 had to be sacrificed.

Fig.17A shows mouse 306, which had a good course of infection, with an outer body temperature of 26.95 °C. Fig.17B shows mouse 301, which had to be sacrificed due to weight

loss as well as temperature loss with an outer body temperature of 24.15 °C. In Fig.17C the experimental setting of the FLIR infrared camera, taking twelve pictures in 2 minutes, can be seen.

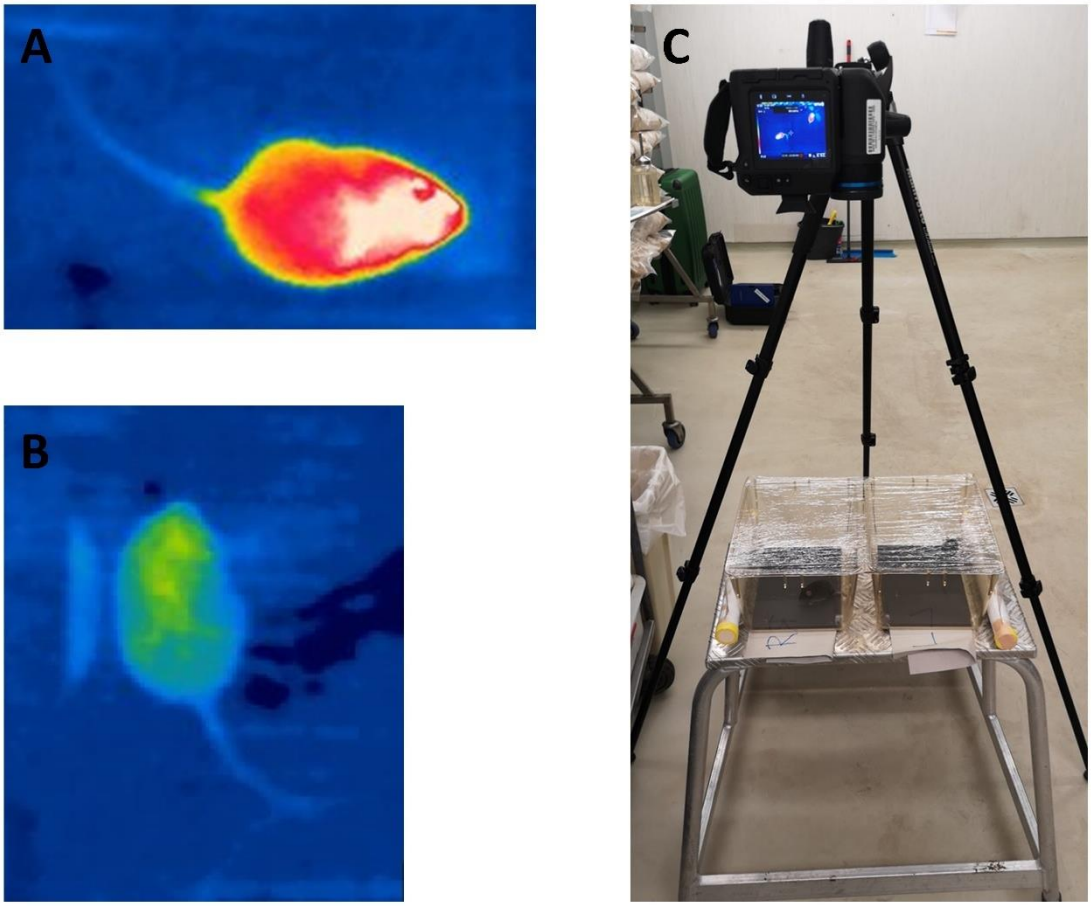

Figure 17: A) Mouse 306, temp. 26.95°C. B) Mouse 301, temp. 24.15°C. C) setting of FLIR camera.

4.9 Comparing the ASF of healthy and MCoV infected mice

Virus induced changes can be observed in the whole body. Therefore, the Altered Schaedler Flora was investigated to observe differences between a healthy and a MCoV infected microbiome. Fig.18 shows qPCR results of the colon DNA samples of clean and healthy mice compared to the MCoV infected mice. The specific targets of the ASF can be seen in Table 16. 500 (*Pseudoflavonifractor sp.*) showed a significant reduction in MCoV infected samples.

Table 16: ASF targets.

356	*Clostridium sp.*
360	*Lactobacillus intestinalis*
361	*Lactobacillus murinus*
457	*Mucispirillum schaedleri*
492	*Eubacterium plexicaudatum*
500	*Pseudoflavonifractor sp.*
502	*Clostridium sp.*
519	*Parabacteroides goldsteinii*
8F & 515R	*Universal 16S rRNA*

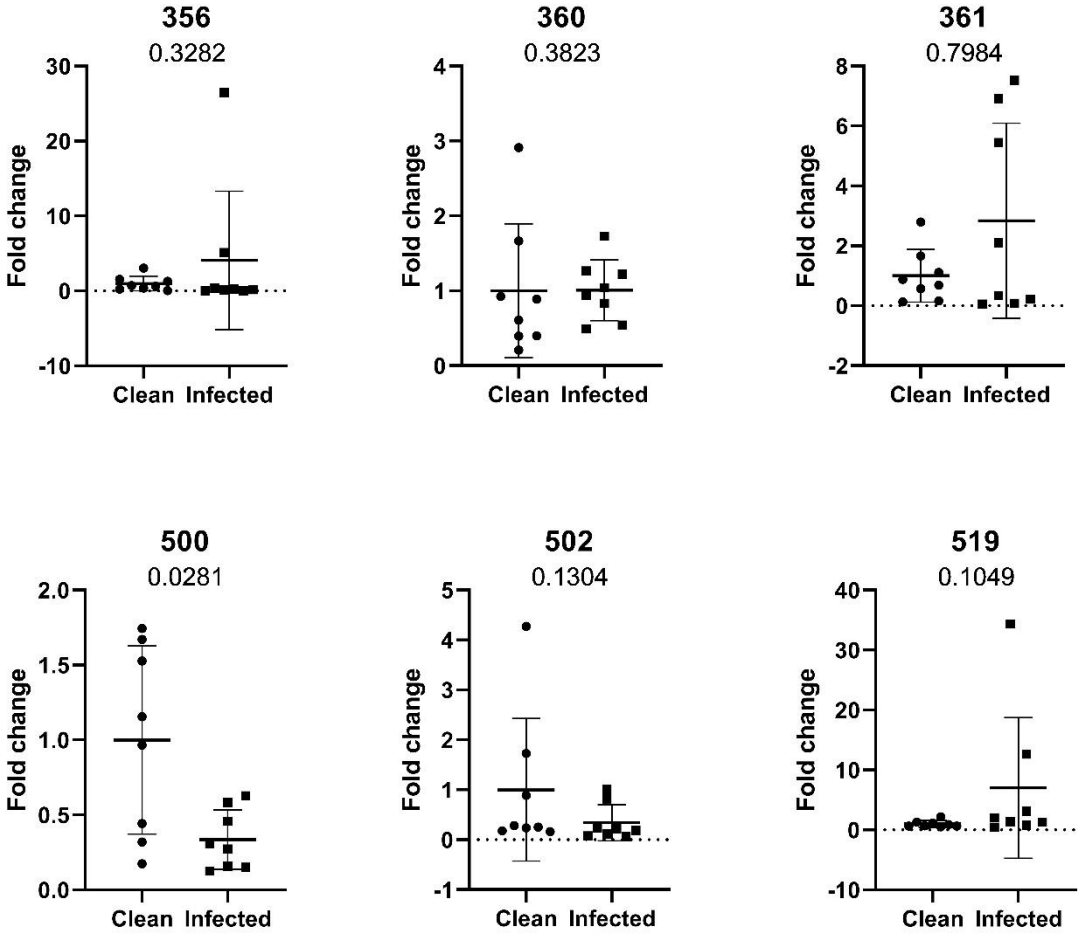

Figure 18:qPCR of colon DNA from clean and M-CoV infected samples. (n=8, mean+/-stdv.)

4.10 Comparing the ASF of the AST and Quarantine mice

As significant differences were observed between healthy and MCoV infected mice the next step was to observe if these changes are MCoV specific or can be generally seen in virus infected mice. Therefore, the next we compared the ASF of mice in the Anna Spiegel

Tierhaltung (AST), which is a specific-pathogen-free (SPF) facility to the cages in the Quarantine facility, both from the Medical University of Vienna. Mice in the Quarantine facility were found to be infected with *Murine Norovirus, Pasteurella sp., Helicobacter sp.* and *Protozoan*. 10-15 feces samples were collected per cage of six cages each condition. Fig.19 shows a significant decrease of 356 and an increase of 361, 502 and 519.

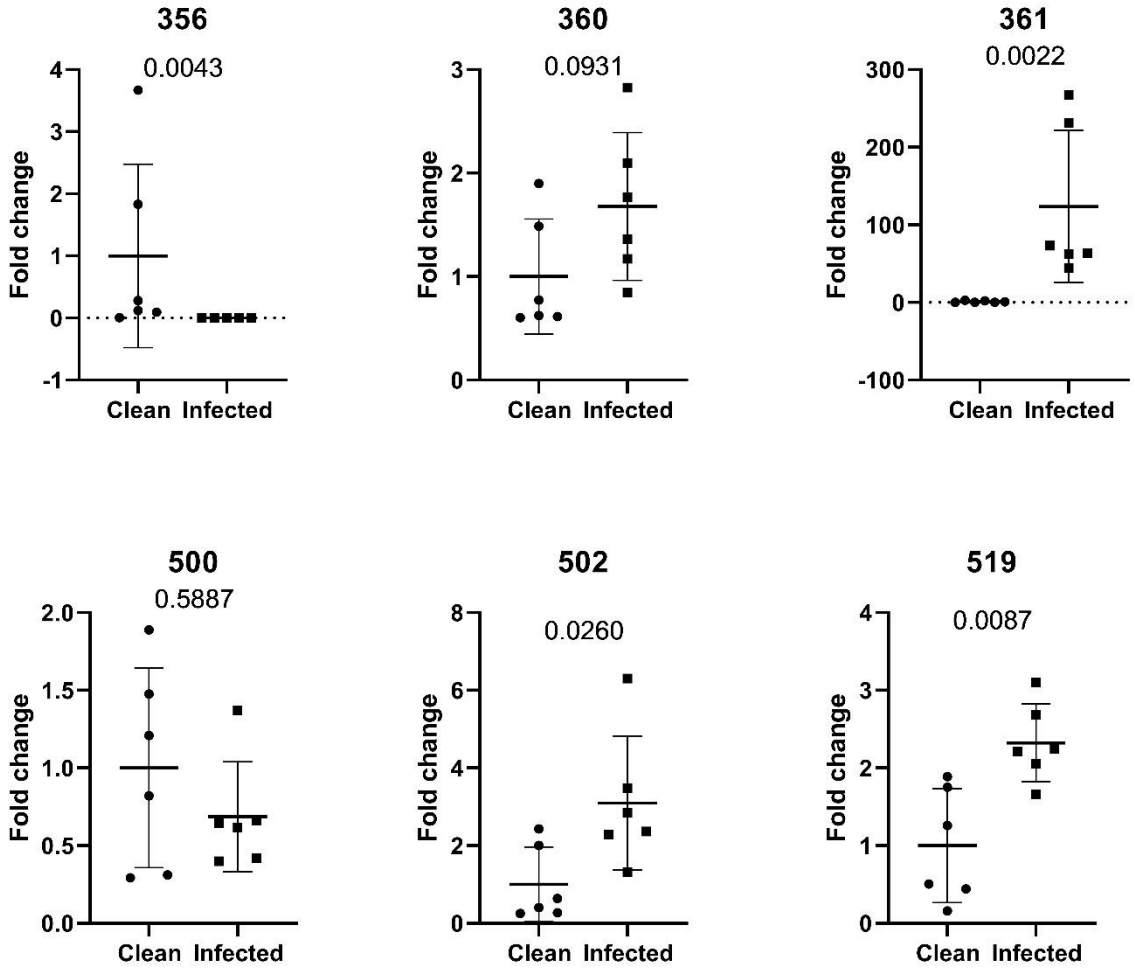

Figure 19: qPCR of AST and Quarantine colon samples. (n=6, mean +/- stdv.)

5 Discussion

To observe the coronavirus induced changes in mouse pathophysiology C57Bl/6J mice were infected with 1.5*10^6 $TCID_{50}$ MCoV. Studies already showed that MCoV is a well-studied coronavirus model affecting lung and liver[1, 13-15]. As the virus causes respiratory disease observing the effects on the lung was the first step where a significant increase of virus burden at day 2 was observed. Another organ to observe was the liver, in which the viral concentration was significantly high at day 4 suggesting that the virus needs some time to migrate from the lung to the liver.

Several studies showed that an infection with SARS-CoV-2 leads to an increased thrombus formation, a higher risk of immunothrombosis and changes in the coagulation system[34, 37]. We observed immunothrombosis in both, lung and liver. In the lung, presence of NETs was highest on day 4. In the liver it was highest at day 2, decreased with day 4 and increased again at day 10. Leading to the question what is happening with the coagulation and the inflammatory system.

To observe the inflammation in the liver, several inflammatory markers like TNFα, IFNγ as well as ICAM-1, VCAM and IFIT-1 and 2 were analyzed. IFIT-1 and IFIT-2 were already high at day 2 and stayed high till day 4. IFNα, TNFα, IFNβ and IFNγ were only high at day 4. ICAM-1, P-selectin, VCAM and Ly6G had a significant increase at day 4 and stayed high till day 10. Results showed in general the highest inflammation rate at day 4. These results lead to the assumption that the antiviral reaction already starts at the moment virus concentration is high in the lung, namely at day 2. High virus burden in the lung at day 2 leads to the first immune reaction in the liver producing IFITs. At day 4, were the virus already reached the whole body and specifically also the liver, IFNs are high and active. At day 4 also other inflammatory markers are significantly increased and stay higher till day 10 until the virus infection is resolved by the immune system.

Exactly this pro-inflammatory reaction of the innate immune system leads to pro-inflammatory and anti-viral cytokine production and further to cytokine production which can cause organ failure including lung and liver and can lead to clot formation and thrombosis [13, 28-30].

Also, fibrinolytic factors like PAI-1, PLG and uPA were analyzed. Studies showed that PAI-1 gets activated and upregulated during and COVID-19 infection[59]. Our results showed a significant increase of PAI-1 and uPA at day 4 whereas no differences in PLG were observed.

The high fold change leads to the assumption, that the low thrombus formation on day 4 in the liver is correlated with the changes of PAI-1 and uPA. uPA is high as there is a high thrombus formation and plasmin needs to be generated to degrade fibrin and further the thrombus, whereas PAI-1 is already working against uPA and trying to block it to stop the thrombus degradation. This is the normal fibrinolytic pathway to dissolve thrombi as described in chapter 1.8[47].

To investigate if these effects of PAI-1 and uPA are inflammation specific an *ex vivo* organ culture was started, where healthy tissue was incubated with TNFα, IL-4 and IFNγ and the fold change of PAI-1, PLG and uPA was determined. With this *ex vivo* set-up, results similar to the *in vivo* situation were generated. uPA was significantly high in all conditions and PAI in the TNFα setting. TGFβ is significantly high in the IFNγ setting and needs to be done for the TNFα stimulation. TNFα and IFNγ are associated with inflammation and studies show upregulated PAI-1 as well as uPA[28, 59, 60].

We also detected collagen formation in lung and liver. Collagen in the lung showed the highest level at day four whereas collagen in the liver was highest at day ten. Showing again that changes first occur in the lung and then in the liver. Studies showed that collagen resulting from fibrosis was found in patients after an infection and could also be signs of long-lasting symptoms[61].

To observe how specific and strong the immune system reacts to the virus, a low dose infection was done where only a $TCID_{50}$ of 1400 was used. Results show that even with this low dose, there is a strong immune reaction of the adaptive immune system as already at day 2, T-cell and macrophage activity can be observed even though the viral load is so low that it cannot be detected anymore with a qPCR. Studies showed in mild stages of COVID-19 in patients that a significant higher lymphocyte count was found as well as CD3+ and CD8+ T-cell populations[27], which is in line with our results.

MCoV does not only have an influence on the immune system and the organs but also on the body temperature, the wellbeing, and the weight of mice. As already described, monitoring of the body temperature is a standard procedure in patients as well as animals and animal models during experiments[48-50]. Therefore, with the help of the FLIR infrared camera, which is a non-invasive method, it was observed if the outer body temperature is a better or earlier indicator for the sickness of mice than the weight. Results show that weight reduction is earlier

than the body temperature change. In severe cases, the weight and temperature loss go simultaneously but in less severe cases a weight loss without a temperature loss was observed and due to 3R and the humane endpoints, mice had to be sacrificed after losing more than 20 % of their starting weight. The experiment led to the finding that with the help of the temperature the mouse wellbeing can be observed, still the experimental endpoints need to be defined depending on the weight. But it was also seen that with the infrared camera a “point of no return” can be defined. If a mouse has an outer body temperature below 24.5 °C it will most probably not recover anymore.

A further impact of MCoV is the change in the microbiome as measured here via the components of the Altered Schaedler Flora, a defined microbiome consisting of eight bacteria, which can be used to study the host-microbe relationship [55, 57]. The microbiome of MCoV infected mice was compared that of healthy mice and showed a significant reduction of 500 *Pseudoflavonifractor sp.*, showing changes of the microbiome due to the infection. To observe, if the qPCR method targeting only ASF can be used to investigate the wellbeing of mice in different conditions and housings, we compared the ASF composition of mice in the AST with mice from a SPF facility where it was known that the animals are infected with *Murine Norovirus, Pasteurella sp., Helicobacter sp.* and *Protozoans*. Our esults show a significand decrease of 356 *Clostirdium sp.* and a significant increase of 361 *Lactobacillus murinus*, 502 *Clostridium sp.*, 519 *Parabacteroides goldsteinii*. This leads to the assumption that animals can be easily compared and their health status can by determined by a targeted qPCR, if there is a known clean standard to compare them to. Different infections can be observed by changes in the microbiome by just observing eight different qPCR targets from the ASF.

6 Summary English

For this master thesis C57BL/6 mice were infected intranasally with the murine coronavirus, which is a great model for SARS-CoV-2 as they are closely related. Our results showed an organ specific difference including the virus burden as highest values in lung can be observed at day 2 and in liver at day 4. NET formation in the lung was highest at day 4 whereas in the liver thrombi can be found already at day 2, at lower numbers at day 4 and again at higher numbers at day 10. This observation led to investigation of the interacting partners in the coagulation cascade where high levels of PAI-1 and uPA were found on day 4. Further the inflammation response in the liver was analyzed as well as an *ex vivo* liver organ culture was established underlining the *in vivo* results. A low dose infection was carried out showing a strong immune response of T-cells and macrophages without any detectable virus. Furthermore, outer body temperature was measured with an infrared camera, and compared to the weight loss during an infection. The microbiome especially the ASF in MCoV infected mice was investigated and compared to healthy mice as well as the ASF of mice in quarantine was compared to mice in a SPF housing. Leading to the results that with a qPCR targeting ASF members and a defended, clean status, alterations in the ASF show infections in mice.

7 Summary German

Diese Arbeit umfasst Ergebnisse von C57Bl/6 Mäuse welche nasal mit einem Mäusecoronavirus, welcher ein gutes Modell für eine Infektion mit SARS-CoV-2 darstellt, infiziert worden sind. Der Mäusecoronavirus ist ein Betacoronavirus und mit SARS-CoV-1 und 2 verwandt. Die Ergebnisse dieser Arbeit zeigen organspezifische Unterschiede in der Viruslast, da man die höchsten Werte am Tag 2 in der Lunge und an Tag 4 in der Leber sehen konnte. Die NET Bildung in der Lunge war am Tag 4 am höchsten, wobei in der Leber Thromben am Tag 2 und 10 gefunden werden konnten. Am Tag 4 war die Anzahl der Thromben in der Leber signifikant geringer. Diese Beobachtung führte zur Untersuchung von Interaktionspartnern in dem Gerinnungssystem, bei der hohe Werte von PAI-1 und uPA am Tag 4 beobachtet wurden. Weiters wurde der Entzündungsprozess in der Leber untersucht und eine Organkultur etabliert, welche die Resultate der *in vivo* Experimente *ex vivo* bestätigte. Die äußere Körpertemperatur wurde mit einer Infrarotkamera gemessen und mit dem Gewichtsverlust im Laufe einer Infektion verglichen. Das Mikrobiom, vor allem die ASF, von MCoV infizierten Mäusen wurde mit Kontrollmäusen verglichen, genauso wie das ASF von Mäusen aus der Quarantäne mit dem von Mäusen aus der SPF Haltung verglichen wurden. Die Ergebnisse zeigten, dass mithilfe einer qPCR und einem definierten sauberen Mikrobiom, Statusänderungen der ASF auf eine Infektion in Mäusen hinweisen können.

8 List of Abbreviations

Acute respiratory distress syndrome	ARDS
Alterd Schaedler Flora	ASF
Angiotensin-converting enzyme 2	ACE2
Anna Spiegel Tierhaltung	AST
Citrullinated histone H4	CitH4
Coronavirus disease 2019	COVID-19
Damage associated molecular patterns	DAMPs
Factor V	FV
Factor X	FX
Gastrointestinal	GI
Infrared Thermography	IRT
Interferon alpha	IFNα
Interferon beta	IFNβ
Interferon gamma	IFNγ
Interferon Induced Protein with Tetratricopeptide Repeats 1	IFIT-1
Interferon Induced Protein with Tetratricopeptide Repeats 2	IFIT-2
Interferons	IFNs
Interleukin-1β	IL-1β
Interleukin-4	IL-4
Intracellular adhesion molecule 1	ICAM-1
Lymphocyte antigen 6 complex locus G6D	Ly6G
Major histocompatibility complex	MHC
Murine coronavirus	MCoV
Murine hepatitis virus	MHV
Myeloperoxidase	MPO
Neutrophil extracellular trap	NET
Pathogen associated molecular patterns	PAMPs
Pathogen recognition receptor	PRR
Plasminogen activator inhibitor 1	PAI-1
Plasminogen activator inhibitor 1	PLG
Receptor binding domain	RBD
Severe acute respiratory syndrome coronavirus	SARS-CoV
Severe acute respiratory syndrome coronavirus 2	SARS-CoV-2
Specific pathogen free	SPF
Tissue factor	TF
Tissue plasminogen activator	tPA
Tumor necrosis factor alpha	TNFα
Urokinase plasminogen activator	uPA
Vascular cell adhesion molecule	VCAM
4′,6-diamidino-2-phenylindole	DAPI

9 Summary of References

1. Korner, R.W., et al., *Of Mice and Men: The Coronavirus MHV and Mouse Models as a Translational Approach to Understand SARS-CoV-2.* Viruses, 2020. **12**(8).
2. Quraishi, M., S.K. Upadhyay, and A. Nigam, *COVID-19 Diagnostics: A Panoramic View on Its Present Scenario, Challenges and Solutions.* Proc Natl Acad Sci India Sect B Biol Sci, 2022: p. 1-13.
3. Harrison, A.G., T. Lin, and P. Wang, *Mechanisms of SARS-CoV-2 Transmission and Pathogenesis.* Trends Immunol, 2020. **41**(12): p. 1100-1115.
4. WHO. 2022 [cited 2022 July]; Available from: https://covid19.who.int/.
5. Dagotto, G., J. Yu, and D.H. Barouch, *Approaches and Challenges in SARS-CoV-2 Vaccine Development.* Cell Host Microbe, 2020. **28**(3): p. 364-370.
6. Dai, L. and G.F. Gao, *Viral targets for vaccines against COVID-19.* Nat Rev Immunol, 2021. **21**(2): p. 73-82.
7. Wang, M.Y., et al., *SARS-CoV-2: Structure, Biology, and Structure-Based Therapeutics Development.* Front Cell Infect Microbiol, 2020. **10**: p. 587269.
8. V'Kovski, P., et al., *Coronavirus biology and replication: implications for SARS-CoV-2.* Nat Rev Microbiol, 2021. **19**(3): p. 155-170.
9. Weiss, S.R. and S. Navas-Martin, *Coronavirus pathogenesis and the emerging pathogen severe acute respiratory syndrome coronavirus.* Microbiol Mol Biol Rev, 2005. **69**(4): p. 635-64.
10. Davies, E., et al., *An Overview of SARS-CoV-2 Molecular Diagnostics in Europe.* Clin Lab Med, 2022. **42**(2): p. 161-191.
11. Schoch, C.L., et al., *NCBI Taxonomy: a comprehensive update on curation, resources and tools.* Database (Oxford), 2020. **2020**.
12. Cheever, F.S., J.B. Daniels, and et al., *A murine virus (JHM) causing disseminated encephalomyelitis with extensive destruction of myelin.* J Exp Med, 1949. **90**(3): p. 181-210.
13. Salzmann, M., et al., *Innate Immune Training with Bacterial Extracts Enhances Lung Macrophage Recruitment to Protect from Betacoronavirus Infection.* J Innate Immun, 2021: p. 1-13.
14. Barthold, S.W. and A.L. Smith, *Response of genetically susceptible and resistant mice to intranasal inoculation with mouse hepatitis virus JHM.* Virus Res, 1987. **7**(3): p. 225-39.
15. Barthold, S.W. and A.L. Smith, *Mouse hepatitis virus strain--related patterns of tissue tropism in suckling mice.* Arch Virol, 1984. **81**(1-2): p. 103-12.
16. Barthold, S.W., D.S. Beck, and A.L. Smith, *Enterotropic coronavirus (mouse hepatitis virus) in mice: influence of host age and strain on infection and disease.* Lab Anim Sci, 1993. **43**(4): p. 276-84.
17. Homberger, F.R., L. Zhang, and S.W. Barthold, *Prevalence of enterotropic and polytropic mouse hepatitis virus in enzootically infected mouse colonies.* Lab Anim Sci, 1998. **48**(1): p. 50-4.
18. Barthold, S.W., M.S. de Souza, and A.L. Smith, *Susceptibility of laboratory mice to intranasal and contact infection with coronaviruses of other species.* Lab Anim Sci, 1990. **40**(5): p. 481-5.
19. Barthold, S.W. and A.L. Smith, *Virus strain specificity of challenge immunity to coronavirus.* Arch Virol, 1989. **104**(3-4): p. 187-96.

20. Barthold, S.W. and A.L. Smith, *Duration of challenge immunity to coronavirus JHM in mice.* Arch Virol, 1989. **107**(3-4): p. 171-7.
21. Vardhana, S.A. and J.D. Wolchok, *The many faces of the anti-COVID immune response.* J Exp Med, 2020. **217**(6).
22. Platanias, L.C., *Mechanisms of type-I- and type-II-interferon-mediated signalling.* Nat Rev Immunol, 2005. **5**(5): p. 375-86.
23. Lee, A.J. and A.A. Ashkar, *The Dual Nature of Type I and Type II Interferons.* Front Immunol, 2018. **9**: p. 2061.
24. Zhou, H. and S. Perlman, *Mouse hepatitis virus does not induce Beta interferon synthesis and does not inhibit its induction by double-stranded RNA.* J Virol, 2007. **81**(2): p. 568-74.
25. Laboratory, T.J. *C57BL/6J*. 2022 [cited 2022 02.07.2022]; Available from: https://www.jax.org/strain/000664?featured.
26. Jarnagin, K., et al., *Animal models for SARS-Cov2/Covid19 research-A commentary.* Biochem Pharmacol, 2021. **188**: p. 114543.
27. Paces, J., et al., *COVID-19 and the immune system.* Physiol Res, 2020. **69**(3): p. 379-388.
28. Celardo, I., et al., *The immune system view of the coronavirus SARS-CoV-2.* Biol Direct, 2020. **15**(1): p. 30.
29. Long, E.O., *ICAM-1: getting a grip on leukocyte adhesion.* J Immunol, 2011. **186**(9): p. 5021-3.
30. Yonekawa, K. and J.M. Harlan, *Targeting leukocyte integrins in human diseases.* J Leukoc Biol, 2005. **77**(2): p. 129-40.
31. Alberts, B., *Molecular biology of the cell*. Sixth edition. ed. 2015, New York, NY: Garland Science, Taylor and Francis Group. 1 volume (various pagings).
32. Andreatta, M., et al., *A CD4(+) T cell reference map delineates subtype-specific adaptation during acute and chronic viral infections.* Elife, 2022. **11**.
33. Al-Kuraishy, H.M., et al., *Neutrophil Extracellular Traps (NETs) and Covid-19: A new frontiers for therapeutic modality.* Int Immunopharmacol, 2022. **104**: p. 108516.
34. Ackermann, M., et al., *Patients with COVID-19: in the dark-NETs of neutrophils.* Cell Death Differ, 2021. **28**(11): p. 3125-3139.
35. Barnes, B.J., et al., *Targeting potential drivers of COVID-19: Neutrophil extracellular traps.* J Exp Med, 2020. **217**(6).
36. Zuo, Y., et al., *Neutrophil extracellular traps in COVID-19.* JCI Insight, 2020. **5**(11).
37. Yaqinuddin, A., *Neutrophil extracellular traps and thrombogenesis in COVID-19 patients.* J Res Med Sci, 2021. **26**: p. 96.
38. Thalin, C., et al., *Neutrophil Extracellular Traps: Villains and Targets in Arterial, Venous, and Cancer-Associated Thrombosis.* Arterioscler Thromb Vasc Biol, 2019. **39**(9): p. 1724-1738.
39. Hisada, Y., et al., *Neutrophils and neutrophil extracellular traps enhance venous thrombosis in mice bearing human pancreatic tumors.* Haematologica, 2020. **105**(1): p. 218-225.
40. Zhang, H., et al., *Histopathologic Changes and SARS-CoV-2 Immunostaining in the Lung of a Patient With COVID-19.* Ann Intern Med, 2020. **173**(4): p. 324.
41. Li, D., et al., *COVID-19-associated liver injury: from bedside to bench.* J Gastroenterol, 2021. **56**(3): p. 218-230.

42. Gaertner, F. and S. Massberg, *Blood coagulation in immunothrombosis-At the frontline of intravascular immunity.* Semin Immunol, 2016. **28**(6): p. 561-569.
43. Antoniak, S., *The coagulation system in host defense.* Res Pract Thromb Haemost, 2018. **2**(3): p. 549-557.
44. Yun, S.H., et al., *Platelet Activation: The Mechanisms and Potential Biomarkers.* Biomed Res Int, 2016. **2016**: p. 9060143.
45. Chapin, J.C. and K.A. Hajjar, *Fibrinolysis and the control of blood coagulation.* Blood Rev, 2015. **29**(1): p. 17-24.
46. Geiger, M., *Fundamentals of Vascular Biology*. 2019: Springer Nature Switzerland. 389.
47. Cesarman-Maus, G. and K.A. Hajjar, *Molecular mechanisms of fibrinolysis.* Br J Haematol, 2005. **129**(3): p. 307-21.
48. Giannetto, C., et al., *Thermographic ocular temperature correlated with rectal temperature in cats.* J Therm Biol, 2021. **102**: p. 103104.
49. Blenkus, U., et al., *Non-Invasive Assessment of Mild Stress-Induced Hyperthermia by Infrared Thermography in Laboratory Mice.* Animals (Basel), 2022. **12**(2).
50. Burkholder, T., et al., *Health Evaluation of Experimental Laboratory Mice.* Curr Protoc Mouse Biol, 2012. **2**: p. 145-165.
51. Redaelli, V., et al., *A refinement approach in a mouse model of rehabilitation research. Analgesia strategy, reduction approach and infrared thermography in spinal cord injury.* PLoS One, 2019. **14**(10): p. e0224337.
52. Brzezinski, R.Y., et al., *Non-invasive thermal imaging of cardiac remodeling in mice.* Biomed Opt Express, 2019. **10**(12): p. 6189-6203.
53. Brzezinski, R.Y., et al., *Automated thermal imaging for the detection of fatty liver disease.* Sci Rep, 2020. **10**(1): p. 15532.
54. Konieczka, K., et al., *Cornea Thermography: Optimal Evaluation of the Outcome and the Resulting Reproducibility.* Transl Vis Sci Technol, 2018. **7**(3): p. 14.
55. Gomes-Neto, J.C., et al., *A real-time PCR assay for accurate quantification of the individual members of the Altered Schaedler Flora microbiota in gnotobiotic mice.* J Microbiol Methods, 2017. **135**: p. 52-62.
56. Brestoff, J.R. and D. Artis, *Commensal bacteria at the interface of host metabolism and the immune system.* Nat Immunol, 2013. **14**(7): p. 676-84.
57. Wymore Brand, M., et al., *The Altered Schaedler Flora: Continued Applications of a Defined Murine Microbial Community.* ILAR J, 2015. **56**(2): p. 169-78.
58. Biggs, M.B., et al., *Systems-level metabolism of the altered Schaedler flora, a complete gut microbiota.* ISME J, 2017. **11**(2): p. 426-438.
59. Huang, P., et al., *A Vicious Cycle: In Severe and Critically Ill COVID-19 Patients.* Front Immunol, 2022. **13**: p. 930673.
60. Wohlrab, P., et al., *Oxygen conditions oscillating between hypoxia and hyperoxia induce different effects in the pulmonary endothelium compared to constant oxygen conditions.* Physiol Rep, 2021. **9**(3): p. e14590.
61. Wiech, M., et al., *Remodeling of T Cell Dynamics During Long COVID Is Dependent on Severity of SARS-CoV-2 Infection.* Front Immunol, 2022. **13**: p. 886431.

10 Summary of Figures

Figure 1: Coronaviridae taxonomy[11]. 1
Figure 2: Overview of the coagulation cascade. The cascade can be divided into 3 parts: the intrinsic, extrinsic and common pathway. The intrinsic pathway is activated by contact whereas the extrinsic is activated by tissue factor (TF). The common pathway is activated by FX coming from either intrinsic or extrinsic pathway. Figure is taken from Fundamentals of Vascular Biology (Fig.8.3).[46] 8
Figure 3: Fibrinolysis pathway. Plasminogen gets converted to Plasmin by the enzymes uPA and tPA which further leads to Fibrin being degraded. Created with BioRender. 9
Figure 4: Experimental setup of the organ culture. Liver from Bl6 mice were taken, cut in small pieces and incubated for 6h in different conditions. Created with BioRender. 17
Figure 5: FLIR temperature picture showing 2 mice which can be measured simultaneously in 2 separate cages. 20
Figure 6: A) qPCR of the virus burden in mice lung at day 2, day 4 and day 10. B) CitH4 staining for NET formation in lung at day 2, day 4 and day 10. Data normalized to day 2. Statistics done with t-test. (n=10, mean+/-stdv) 23
Figure 7: DAPI, MPO and CitH4 staining of a lung thrombus with a merged CitH4 positive thrombus in the mouse lung. 24
Figure 8: A) Virus burden in mice liver at day 2, day4, day10. B) NET formation in liver at day 2, day 4, day 10. Data normalized to day 2. Statistics done with t-test. (n=10, mean +/- stdv.) 25
Figure 9: DAPI, MPO and CitH4 staining of a liver thrombus with a merged CitH4 positive thrombus in the mouse liver. 26
Figure 10: qPCR results of several inflammation markers in the liver. Data is normalized to basal. Statistical analysis was done with a t-test. (n=10, mean+/-stdv.) 27
Figure 11: qPCR of PAI-1, PLG and uPA at basal, day 2, day 4, day 10, showing sign. increase at day4 in B and C but no difference in A. (n=10, mean+/-stdv.) 28
Figure 12: PLG, uPA, PAI and TGFb levels of liver in organ culture for 6h with 3 different concentrations of TNFa, IL4 and IFN-y(n=5, mean+/-stdv.) 30
Figure 13:Trichrome staining of collagen in lung and liver and qPCR of prothrombin. (Basal n=7 Day2,4,10 n=10, mean+/-stdv.) 31
Figure 14: Trichrome staining of A) liver B) lung. Blue indicating collagen. 32
Figure 15: Low concentration M-CoV infection in the lung showing B-cells, T-cells and macrophages. (n=7 control, n=5 MHV, mean+/-stdv.) 33
Figure 16: Grouped temperature and weight measured AM and PM for ten days. Mouse 306 and 301 survived, mouse 308 had to be sacrificed. 34
Figure 17: A) Mouse 306, temp. 26.95°C. B) Mouse 301, temp. 24.15°C. C) setting of FLIR camera. 35
Figure 18:qPCR of colon DNA from clean and M-CoV infected samples. (n=8, mean+/-stdv.) 36
Figure 19: qPCR of AST and Quarantine colon samples. (n=6, mean +/- stdv.) 37

11 Summary of Tables

Table 1: The eight members of the altered Schaedler flora (ASF).....11
Table 2: qPCR Mastermix for virus burden in lung and liver.....13
Table 3: qPCR Targets for virus burden in lung and liver.....14
Table 4: qPCR protocol for virus burden in lung and liver.....14
Table 5:qPCR Mastermix for inflammation, PAI, PLG and uPA.....15
Table 6: qPCR Targets for inflammation, PAI, PLG and uPA.....16
Table 7: qPCR protocol for inflammation, PAI, PLG and uPA.....16
Table 8: qPCR Mastermix for organ culture samples.....17
Table 9: qPCR targets for organ culture samples.....18
Table 10: qPCR protocol for organ culture samples.....18
Table 11: T-cell mix for flow cytometry.....19
Table 12: Monocytes and macrophages mix for flow cytometry.....20
Table 13: qPCR targets microbiome.....21
Table 14: qPCR Mastermix for microbiome.....21
Table 15: qPCR protocol for microbiome.....22
Table 16: ASF targets.....36